European Journal of Medicinal Chemistry 46 (2011) 4489–4505

Contents lists available at ScienceDirect

European Journal of Medicinal Chemistry

journal homepage: http://www.elsevier.com/locate/ejmech

Original article

Homology modeling in tandem with 3D-QSAR analyses: A computational approach to depict the agonist binding site of the human CB2 receptor

Elena Cichero [a], Alessia Ligresti [b], Marco Allarà [b], Vincenzo di Marzo [b], Zelda Lazzati [c,d], Pasqualina D'Ursi [c], Anna Marabotti [c], Luciano Milanesi [c], Andrea Spallarossa [a], Angelo Ranise [a], Paola Fossa [a,*]

[a] Dipartimento di Scienze Farmaceutiche, Università di Genova, Viale Benedetto XV n. 3, 16132 Genova, Italy
[b] Endocannabinoid Research Group, Istituto di Chimica Biomolecolare, CNR, Via Campi Flegrei 34, 80078 Pozzuoli Napoli, Italy
[c] Institute for Biomedical Technologies – National Research Council (ITB-CNR), Via Fratelli Cervi 93, 20090 Segrate (MI), Italy
[d] Institute of Genetics and Biophysics "A. Buzzati Traverso" – National Research Council (IGB-CNR), Via P. Castellino 111, 80131 Naples, Italy

ARTICLE INFO

Article history:
Received 8 November 2010
Received in revised form
14 July 2011
Accepted 14 July 2011
Available online 23 July 2011

Keywords:
Cannabinoid receptor
CB2 agonist
Homology modeling
3D-QSAR
CoMSIA
MD simulations

ABSTRACT

CB2 receptor belongs to the large family of G-protein coupled receptors (GPCRs) controlling a wide variety of signal transduction. The recent crystallographic determination of human β2 adrenoreceptor and its high sequence similarity with human CB2 receptor (*h*CB2) prompted us to compute a theoretical model of *h*CB2 based also on β2 adrenoreceptor coordinates. This model has been employed to perform docking and molecular dynamic simulations on **WIN-55,212-2** (CB2 agonist commonly used in binding experiments), in order to identify the putative CB2 receptor agonist binding site, followed by molecular docking studies on a series of indol-3-yl-tetramethylcyclopropyl ketone derivatives, a novel class of potent CB2 agonists. Successively, docking-based Comparative Molecular Fields Analysis (CoMFA) and Comparative Molecular Similarity Indices Analysis (CoMSIA) studies were also performed. The CoMSIA model resulted to be the more predictive, showing $r^2_{ncv} = 0.96$, $r^2_{cv} = 0.713$, SEE = 0.193, $F = 125.223$, and $r^2_{pred} = 0.78$. The obtained 3D-QSAR models allowed us to derive more complete guidelines for the design of new analogues with improved potency so as to synthesize new indoles showing high CB2 affinity.

1. Introduction

Cannabinoid receptors interact with cannabinoid drugs including the classical cannabinoids, such as Δ^9- tetrahydrocannabinol (Δ^9-THC), their synthetic analogues and the endogenous cannabinoids [1–4]. Currently, two subtypes of cannabinoid receptors have been cloned and pharmacologically characterized, the cannabinoid 1 receptor (CB1) and the cannabinoid 2 receptor (CB2), even if at present their is some experimental evidence that supports the existence of additional types of cannabinoid receptors [5–7]. CB1 is mainly located within the central nervous system (CNS) at presynaptic nerve terminals, while CB2 is mainly associated with immune system cells. Thus, CB2 selective compounds had been described in the literature to be active in different neuropathic and inflammatory pain models [8–12]. Since CB2 receptors had been found recently in CNS tissues showing some neuroprotective roles, CB2 agents could also be applied in the prevention of some neurodegenerative disorders, such as Huntington and Alzheimer's diseases [13–15]. Other studies have also highlighted potential roles for CB2 in cancer [16,17], multiple sclerosis [18] and bone regeneration [19,20]. Since CB2 is expressed mainly on immune tissues, selective CB2 agonists appear to be devoid of central effects attributable to CB1 activation.

Both CB1 and CB2 belong to the large family of G-protein coupled receptors (GPCRs) [21] controlling a wide variety of signal transduction. Since GPCR are membrane proteins, their expression, purification, crystallization and structure determination present major challenges to the discovery of new drugs. In the absence of experimental data about human cannabinoid receptor 3D structures, computer–aided GPCR-targeted drug design can be performed on the basis of homology modeling techniques in tandem with ligand-based modeling strategies, such as 3D-QSAR analyses.

Up to now, various computer generated molecular models of ligand-CB2 complexes have been built and evaluated, some of the latest being those developed by Salo, Tuccinardi and, more recently by Durdagi [22]. In the present work, with the aim of gaining a better

* Corresponding author. Tel.: +39 010 3538238; fax: +39 010 3538358.
E-mail address: fossap@unige.it (P. Fossa).

0223-5234/$ – see front matter © 2011 Elsevier Masson SAS. All rights reserved.
doi:10.1016/j.ejmech.2011.07.023

understanding of the agonist-CB2 receptor interactions and in particular to outline specific CB2 agonists binding mode, a theoretical model of the human CB2 receptor (*h*CB2) has been built taking into account the human β2 adrenoreceptor [23], human A2A adenosine receptor [24] and rhodopsin bovine coordinates [25].

This model has been refined by docking and molecular dynamic simulations on **WIN-55,212-2** (CB2 agonist commonly used in binding experiments; $pK_i = 8.89$) in order to identify the putative CB2 receptor agonist binding site.

Successively, in order to assess the reliability of the protein model built as a tool for virtual screening procedures, we performed docking simulations on a series of indol-3-yl-tetramethylcyclopropyl ketone derivatives, a novel class of potent CB2 agonists [26] (in Fig. 1, compound **17** as representative indol-3-yl-tetramethylcyclopropyl ketone and **WIN-55,212-2** are depicted). Furthermore, docking-based Comparative Molecular Fields Analysis (CoMFA) and Comparative Molecular Similarity Indices Analysis (CoMSIA) studies could provide a complementary tool for drug design. Thus, on the same set of indol-3-yl-tetramethylcyclopropyl ketone derivatives, 3D-QSAR studies were also performed. The obtained CoMFA and CoMSIA maps, offered useful suggestions for the design of new indol-3-yl-tetramethylcyclopropyl ketones with improved potency and also allowed us to synthesize four new indoles showing high CB2 affinity.

2. Materials and methods

2.1. Data set

A dataset of forty-six indol-3-yl-tetramethylcyclopropyl ketones derivatives, screened according to the same pharmacological protocol, were selected from literature [26]. Compounds **1**–**46** (Table 1) and **WIN-55,212-2** have been built, parameterized (Gasteiger-Hückel method) and energy minimized within MOE using MMFF94 force field (the root mean square gradient has been set to 0.00001) [27].

2.2. Human CB2 receptor homology modeling

Since most of the key residues characteristic of GPCRs are conserved in CB2 receptor, a *h*CB2 receptor homology model has been generated, starting from the X-ray structures of human β_2 adrenoreceptor (PDB code: 2RH1; resolution = 2.40 Å), human A2A adenosine receptor (PDB code: 3EML; resolution = 2.60 Å) and rhodopsin bovine (PDB: 1F88, resolution = 2.80 Å), as GPCR templates.

The amino acid sequence of *h*CB2 was retrieved from the SWISSPROT database [28] while the three-dimensional structure coordinates file of the GPCR templates were obtained from the Protein Data Bank [29].

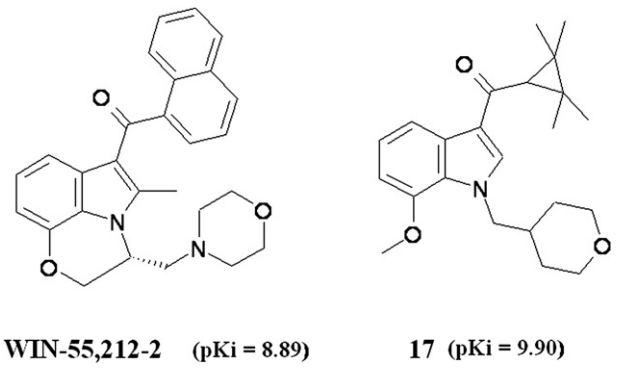

Fig. 1. Chemical structure and pK_i value of CB2 agonists **WIN-55,212-2** and **17**.

Since CB2 receptor contains many of the conserved motifs associated with GPCRs, the amino acid sequences of CB2 TM helices were aligned with the corresponding residues of 2RH1, 3EML and 1F88. Due to the lack of the conserved proline in CB2 transmembrane domain 5, the length of this portion has been determined on the base of hydrophobicity similarity criteria, using the sequence editor tool in MOE software [27].

The connecting loops were constructed by the loop search method implemented in MOE. The protein structure was minimized with MOE using the AMBER94 force field [30]. The energy minimization was carried out by the 1000 steps of steepest descent followed by conjugate gradient minimization until the rms gradient of the potential energy was less than 0.1 kcal mol^{-1} $Å^{-1}$.

2.3. Molecular docking of *WIN-55,212-2*

With the aim of outline specific CB2 agonists binding mode, docking studies had been performed according to the following protocol. Initially, **WIN-55,212-2** (ligand commonly used in binding experiments) was submitted to docking calculation. The ligand was docked into the putative ligand binding site using the flexible docking module implemented in MOE. According to the studies performed by Tuccinardi and co-workers [31], for the *h*CB2 receptor agonist activity, formation of H-bond contacts and π–π interactions with S112 and F197, are necessary. Thus, **WIN-55,212-2** was docked into the putative CB2 binding site, including the residues cited above, as identified by the MOE tool SiteFinder. The compound best-docked pose, evaluated in terms of "London dG", has been refined by energy minimization (MMFF94) and rescored according to "Affinity dG" (kcal/mol of total estimated binding energy). Following this procedure, on the basis of the final docking scoring function (S), we identify the most probable **WIN-55,212-2** confomer interacting with CB2 (lowest mean S value).

To better refine the derived **WIN-55,212-2**/receptor complex, a rotamer exploration of all side chains involved in the agonist binding was carried out, by rotamer explorer module of MOE.

The derived *h*CB2/**WIN-55,212-2** complex model was minimized by CHARMM27 and submitted to molecular dynamics simulations.

2.4. Molecular dynamics simulations

The human CB2 receptor in complex with **WIN-55,212-2** obtained from docking studies has been investigated by means of MD simulations in lipid bilayer formed by POPC molecules to simulate the physiological context of the protein. The starting POPC lipid bilayer system was obtained from Dr. Tieleman's web page http://moose.bio.ucalgary.ca/index.php?page=Structures_and_Topologies and is formed by 128 lipids and 2460 water, equilibrated with 1 ns MD at 300 K [32–34]. It was extended by 2 × 2 × 1 in xyz directions, in order to have a bilayer large enough to ensure that the protein was completely and homogeneously surrounded by lipids.

Molecular dynamic (MD) simulations were performed using GROMACS package version 4.5.3 [35,36], simulations were performed in parallel (MPI) on a Linux Cluster of 32 nodes, each SuperMicro equipped of two processors: the 2.50 Ghz INTEL(R) Quad-core and the 16 GB Xeon(R), for a 256 total processors interconnected with the Infiniband 4× network and 512 GB of RAM. The GROMOS96 43a1 force field [37] modified in order to include Berger's parameters for lipids [38] was used throughout the simulations. The topology for the ligand was created employing the server PRODRG 2.5 Beta [39], but following suggestions of literature data [40], charges were checked and

Table 1
Molecular structure of CB2 ligands **1**–**46**.

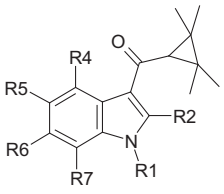

Comp	R1	R2	R4	R5	R6	R7
1	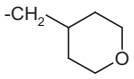	H	F	F	F	F
2	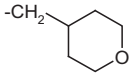	H	H	F	H	H
3	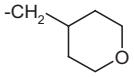	H	H	Cl	H	H
4	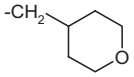	H	H	Br	H	H
5	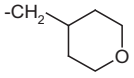	H	H	H	Cl	H
6	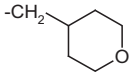	H	H	H	Br	H
7	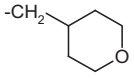	H	H	H	CH_3	H
8	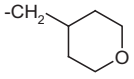	H	H	H	CF_3	H
9	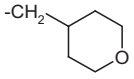	H	H	H	SO_2CH_3	H
10	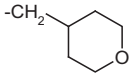	H	OH	H	H	H
11	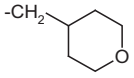	H	H	OH	H	H
12	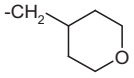	H	H	H	OH	H
13	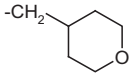	H	H	H	H	OH
14	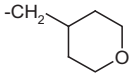	H		H	H	H
15	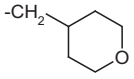	H	H		H	H

(*continued on next page*)

Table 1 (*continued*)

Comp	R1	R2	R4	R5	R6	R7
16	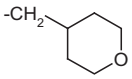	H	H	H		H
17	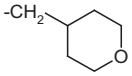	H	H	H	H	
18	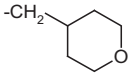	H	OCH_2Ph	H	H	H
19	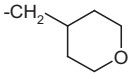	H	H	OCH_2Ph	H	H
20	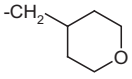	H	H	H	OCH_2Ph	H
21	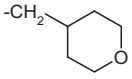	H	H	H	H	OCH_2Ph
22	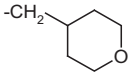	H	H	NH_2	H	H
23	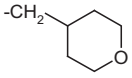	H	H	$O(CH_2)_4OH$	H	H
24	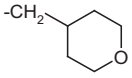	H	H	$O(CH_2)_4Br$	H	H
25	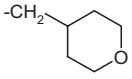	H	H	CN	H	H
26	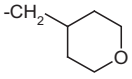	H	H	CH_2OH	H	H
27	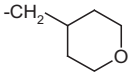	H	H	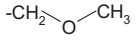	H	H
28	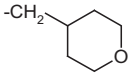	H	H	CO_2CH_3	H	H
29	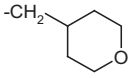	H	H		H	H
30	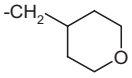	H	H	H	CN	H
31	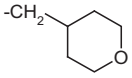	H	H	H	CN_2NH_2	H
32	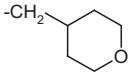	H	H	H	CO_2CH_3	H
33	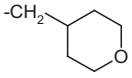	H	H	H		H

Table 1 (*continued*)

Comp	R1	R2	R4	R5	R6	R7
34	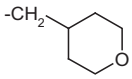	H	H	OCH_2Ph		H
35	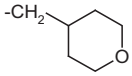	H	H	OH		H
36	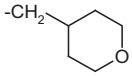	H	H	OH	OH	H
37	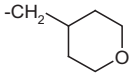	H	H			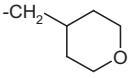
38	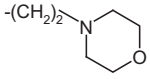	H	H	H	H	H
39	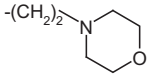	H	H	OH	H	H
40	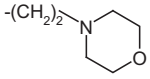	H	H	H	OH	H
41	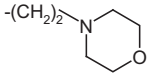	H	H		H	H
42	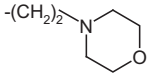	H	H	H		H
43	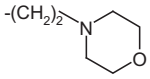	H	H	H	OCH_2Ph	H
44	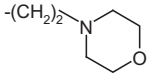	CH_3	H	H	H	H
45	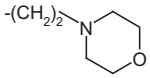	H	NO_2	H	H	H
46	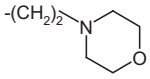	H	NH_2	H	H	H

reassigned using Antechamber program [41] and applying the semiempirical AM1 – bond charge correction (AM1 – BCC) method [42,43]. The CB2 receptor–ligand complex was mildly minimized *in vacuo* in order to reduce steric hindrance, using a Steepest Descent algorithm. The orientation of CB2 receptor–ligand complex regarding to the lipid membrane was checked based on available information in literature [44], and inserted into POPC bilayer using the molecular graphic program VMD [45]. After then, further 19701 water molecules were added to the system, to cover completely the protein by the solvent, and 12 chloride ions were added for neutralization. The coordinates of this system were used as a starting point to insert the protein into the lipid bilayer, with the aid of the newly developed *g_membed* computational tool [46]. *G_membed* first decreases the width of the protein in the x–y plane and remove all molecules (lipids and water) that overlap with the narrowed protein. In our case, only 22 POPC molecules were removed. After that, 1000 MD steps were applied to regrowth the protein to its original size. In order to perform this process, the position of protein + ligand group in the membrane was blocked and the internal protein + ligand interactions were excluded. A cut-off of 1.4 nm was applied to van der Waals interactions and the electrostatic interactions were treated using PME [47] with a real space cut-off of 1.0 nm. All bonds were constraint using the LINCS algorithm [48] allowing a time step of 2 fs. The temperature and pressure were kept constant at 310 K and 1 bar using velocity rescaling [49] and Berendsen semi-isotropic pressure coupling [50]. Periodic boundary conditions were used to exclude surface effects. All these parameters for *g_membed* protocol were kindly provided by Dr. M.G. Wolf (personal communication). After that, the protein + ligand complex embedded in the membrane was submitted to 1 ns MD simulation to equilibrate the system. The settings of these MD

simulations were the same as previously, with the exception that the protein was allowed to move and that the internal protein + ligand interactions were restored. To check for the correct equilibration of the system, we followed the stabilization of the energy of the system, and of the box vectors to ensure that the membrane has a stable lateral area. Finally, the production MD simulation was carried out with the same settings as the equilibration MD, for further 20 ns.

Next, several analyses were conducted using programs built within the GROMACS package, and results were visualized and elaborated with the aid of the freeware program Grace (http://plasmagate.weizmann.ac.il/Grace). The energy components, temperature and pressure, and the box vectors were analyzed to confirm the stabilization of the system. The equilibration of the system was reached after 5 ns of simulation, therefore all analyses were made starting from 5 ns. Visualization and analysis of model features was carried out using VMD [45] and Pymol [51] programs.

To obtain a representative structure for the trajectory, we performed a cluster analysis using GROMACS utilities, with a cut-off of 0.1 nm for RMSD calculation after partial least-square fitting. A single cluster was obtained for the whole trajectory. An average structure was then calculated and minimized using the same protocol described above. The resulting minimized structure of the complex between protein and **WIN-55,212-2** was used as representative structure for the following docking study.

The stereochemistry of the model has been validated through the analysis of Ramachandran plot, by means of Procheck. In order to verify the reliability of the derived receptor model, it has been superimposed and compared to the 2RH1 coordinates (being the template with the higher sequence similarity).

2.5. Molecular docking of compounds **1**–**46**

The final *h*CB2/**WIN-55,212-2** model (obtained by the MD simulations) has been used as starting point for the automatic docking analysis of compounds **1**–**46**. Thus, each compound was docked into the putative CB2 binding site using the flexible docking module implemented in MOE, and refined by minimization with CHARMM27, following the same procedure used for **WIN-55,212-2** docking analysis, as described above. Since both the protein model built and the docking protocol applied proved to be reliable (by properly explaining why compounds **1**–**46** are more or less active as *h*CB2agonists), we performed the following 3D-QSAR analyses on the basis of the compound selected docking poses, which resulted to be aligned into the *h*CB2 putative binding site.

2.6. 3D-QSAR analyses

In tandem with structure-based drug design, the docking-based 3D-QSAR approach of CoMFA [52] and CoMSIA analyses [53] by SybyX 1.0 software [54], could provide a complementary tool for drug design. Thus, the compound selected docking poses, aligned into the *h*CB2 putative binding site, were submitted to 3D-QSAR studies.

2.6.1. Training set and test set

All the compounds were grouped into a training set, for model generation, and a test set, for model validation, containing 37 and 9 compounds respectively. The molecules of the test set represent the 24% (estimated as a good percentage to validate a molecular model) of the training set. Both the training and the test set were divided manually according to a representative range of biological activities and structural variations. For QSAR analysis, K_i values have been transformed into pK_i values and then used as response variables. Compounds receptor affinity covered 4 log orders.

2.6.2. CoMFA and CoMSIA interaction energies

CoMFA method [52] is a widely used 3D-QSAR technique to relate the biological activity of a series of molecules to their steric and electrostatic fields, which are calculated placing the aligned molecules, one by one, into a 3D cubic lattice with a 2 Å grid spacing. The van der Waals potential and Coulombic terms, which represent steric and electrostatic fields, respectively, were calculated using the standard Tripos force field method. The column-filtering threshold value was set to 2.0 kcal/mol to improve the signal-noise ratio. A methyl probe with a +1 charge was used to calculate the CoMFA steric and electrostatic fields. A 30 kcal/mol energy cut-off was applied to avoid infinity of energy values inside the molecule. The CoMSIA method [53] calculates five descriptors, namely steric, electrostatic and hydrophobic parameters, and the H-bond donor and H-bond acceptor properties. The similarity index descriptors were calculated using the same lattice box employed for the CoMFA calculations and a sp^3 carbon as probe atom with a +1 charge, +1 hydrophobicity and +1 H-bond donor and +1 H-bond acceptor properties.

2.6.3. Partial least-square (PLS) analysis and models validation

The partial least-squares (PLS) approach, an extension of the multiple regression analysis, was used to derive the 3D-QSAR models. CoMFA and CoMSIA descriptors were used as independent variables and pEC_{50} values were used as dependent variables. Prior to the PLS analysis, CoMFA and CoMSIA columns with a variance of less than 2.0 kcal mol^{-1} were filtered by using column-filtering to improve the signal-to-noise ratio.

The leave one out (LOO) cross-validation method was used to check the predictivity of the derived model and to identify the optimal number of components (ONC) leading to the highest cross-validated r^2 (r^2_{cv}). In the LOO methodology, one molecule is omitted from the dataset and a model is derived involving the rest of the compounds. Employing this model, the activity of the omitted molecule is then predicted.

The ONC obtained from cross-validation methodology was used in the subsequent regression model. Final CoMFA and CoMSIA models were generated using non-cross-validated PLS analysis. To further assess the statistical confidence and robustness of the derived models, a 100-cycle bootstrap analysis was performed. This is a procedure in which *n* random selections out of the original set of *n* objects are performed several times (100-times were required to obtain a good statistical information). In each run, some objects may not be included in the PLS analysis, whereas some others might be included more then once. The mean correlation coefficient is represented as bootstrap r^2(r^2_{boot}).

2.6.4. Predictive correlation coefficient (r^2_{pred})

To further validate the CoMFA and CoMSIA derived model, the predictive ability for the test set of compounds (expressed as r^2_{pred}) was determined by using the following equation:

$$r^2_{pred} = (SD - PRESS)/SD$$

SD is the sum of the squared deviations between the biological activities of the test set molecules and the mean activity of the training set compounds and PRESS is the sum of the squared deviation between the observed and the predicted activities of the test set compounds.

All calculations were carried out using a PC running the Windows XP operating system and an SGI O2 Silicon Graphics.

2.7. Chemistry

The newly synthesized compounds **48a**–**d** (Table 2) were obtained starting from indoles **47a-b** by alkylation, employing KOH

Table 2
Newly synthesized indoles **48a**–**48d**.

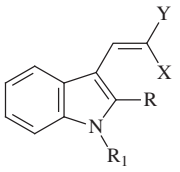

	X	Y	R	R1	Yield
48a	CN	$SO_2C_6H_5$	H	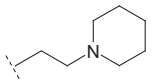	55
48b	COPh	COOEt	H	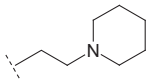	57
48c	CN	$SO_2C_6H_5$	H	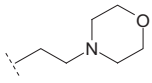	40
48d	COPh	COOEt	H	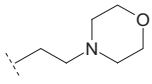	40

as base, Aliquat as phase transfer catalyst and chloroalkylamines as alkylating agents (Scheme 1). The synthesis of compounds **47a-b** was performed starting from indole *via* iminium salt formation and condensation according to the procedure already described [55].

*2.7.1. (2E)-3-(1H-indol-3-yl)-2-(phenylsulfonyl) acrylonitrile (**47a**)*

Yield: 71%; m.p.: 214–216 °C (ethyl acetate). IR (KBr): 3352 (NH), 2210 (CN), 1567 (C=C) 1305 (SO_2), 1140 (SO_2) cm^{-1}. ^1H NMR ($CDCl_3$) δ: 7.26–7.30 (m, 2H, Ar–H), 7.40–7.60 (m, 4H, Ar–H), 7.78–7.83 (m, 1H, Ar–H) 7.94–7.99 (m, 2H, Ar–H), 8.41 (d, J = 3.0 Hz, 1H, indole H-2), 8.47 (s, 1H, CH=C), 9.67 (br s, 1H, NH). Anal. Calcd for $C_{17}H_{12}N_2O_2S$: C, 66.22; H, 3.92; N, 9.08; S, 10.40. Found: C, 65.95; H, 3.67; N, 9.07; S, 10.02.

*2.7.2. Ethyl (2E)-2-benzoyl-3-(1H-indol-3-yl)acrylate (**47b**)*

Yield: 38%; m.p.: 160–163 °C (diethyl ether); IR ($CHCl_3$): 3465 (NH), 2939 (CH_2CH_3), 1705 (COOEt), 1667 (COPh); 1609 (C=C) cm^{-1}. ^1H NMR ($CDCl_3$) δ: 1.09 (t,J = 7.1 Hz, 3H, CH_3), 4.15 (q, J = 7.1 Hz, 2H, CH_2), 7.15–7.38 (m, 6H, Ar–H), 7.42–7.52 (m, 1H, Ar–H), 7.75–7.80 (m, 1H, Ar–H) 7.89–7.94 (m, 2H, A–H), 8.26 (s, 1H, CH=C), 8.71 (br s, 1H, NH). Anal. Calcd for $C_{20}H_{17}NO_3$: C, 75.22; H, 5.37; N, 4.39. Found: C, 75.07; H, 5.69; N, 4.35.

*2.7.3. (E)-2-(phenylsulfonyl)-3-(1-(2-(piperidin-1-yl)ethyl)-1H-indol-3-yl)prop-2-enenitrile(**48a**)*

Yield: 55%; m.p.: 155–156 °C (ethanol); IR (KBr): 2932–2770 (CH_2,CH_3), 2202 (CN), 1566 (C=C), 1340 (SO_2), 1153 (SO_2) cm^{-1}. ^1H NMR (DMSO-d_6) δ: 1.28–1.55 (m, 6H, 3 × CH_2), 2.30–2.48 (m, 4H, 2 × N–CH_2), 2.63 (t, J = 6.9 Hz, 2H, N–CH_2), 4.45 (t, J = 6.9 Hz, 2H, N–CH_2), 7.30–7.42 (m, 2H, Ar–H), 7.67–7.84 (m, 4H, Ar–H), 8.03–8.15 (m, 3H, Ar–H), 8.57 (s, 1H, indole H-2), 8.67 (s, 1H, CH=C). Anal. Calcd for $C_{24}H_{25}N_3O_2S$: C, 68.71; H, 6.01; N, 10.02; S, 7.64. Found: C, 68.92; H, 5.97; N, 9.97; S, 7.74.

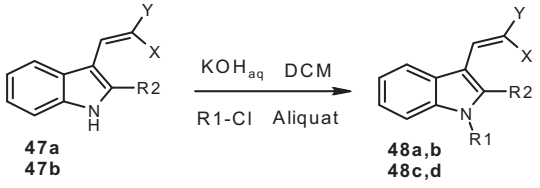

Scheme 1. Synthesis of the compounds **48a**–**d**.

*2.7.4. (E)-ethyl 2-(phenylcarbonyl)-3-(1-(2-(piperidin-1-yl)ethyl)-1H-indol-3-yl)prop-2-enoate (**48b**)*

Yield: 57%; m.p.: 135–138 °C (acetone); IR (KBr): 2943–2762 (CH_2, CH_3), 1705 (COOEt), 1667 (COPh); 1605 (C=C) cm^{-1}. ^1H NMR (DMSO-d_6) δ: 1.12 (t,J = 7.3 Hz, 3H, CH_3), 1.20–1.34 (m, 6H, 3 × CH_2), 2.10–2.29 (m, 4H, 2 × N–CH_2), 2.41 (t, J = 7.0 Hz, 2H, N–CH_2), 4.15 (q, J = 7.3 Hz, 2H, CH_2), 4.35 (t, J = 7.0 Hz, 2H, N–CH_2), 7.18–7.32 (m, 3H, Ar–H), 7.42–7.60 (m, 4H, Ar–H), 7.82–7.90 (m, 1H, Ar–H) 7.91–7.99 (m, 2H, Ar–H), 8.19 (s, 1H, CH=C), Anal. Calcd for $C_{27}H_{30}N_2O_3$: C, 75.32; H, 7.02; N, 6.51. Found: C, 75.64; H, 7.11; N, 6.11.

*2.7.5. (E)-3-(1-(2-morpholinoethyl)-1H-indol-3-yl)-2-(phenylsulfonyl)prop-2-enenitrile (**48c**)*

Yield: 40%; m.p.: 143–145 °C (ethyl acetate); IR (KBr): 2970–2800 (CH_2,CH_3), 2199 (CN), 1561 (C=C), 1332 (SO_2), 1145 (SO_2) cm^{-1}. ^1H NMR (DMSO-d_6) δ: 2.37–2.47 (m, 4H, 2 × N–CH_2), 2.68 (t, J = 6.9 Hz, 2H, N–CH_2), 3.50–3.60 (m, 4H, 2 × O–CH_2), 4.47 (t, J = 6.9 Hz, 2H, N–CH_2), 7.31–7.42 (m, 2H, Ar–H), 7.68–7.83 (m, 4H, Ar–H), 8.00–8.11 (m, 3H, Ar–H), 8.57 (s, 1H, indole H-2), 8.70 (s, 1H, CH=C). Anal. Calcd for $C_{23}H_{23}N_3O_3S$: C, 65.54; H, 5.50; N, 9.97; S, 7.61. Found: C, 65.36; H, 5.70; N, 10.06; S, 7.32.

*2.7.6. (E)-ethyl 3-(1-(2-morpholinoethyl)-1H-indol-3-yl)-2-(phenylcarbonyl)prop-2-enoate (**48d**)*

Yield: 40%; m.p.: 145–147 °C (ethyl acetate); IR (KBr): 2970–2795 (CH_2, CH_3), 1704 (COOEt), 1667 (COPh); 1616 (C=C) cm^{-1}. ^1H NMR (DMSO-d_6) δ: 1.12 (t,J = 7.0 Hz, 3H, CH_3), 2.46 (t, J = 7.1 Hz, 2H, N–CH_2), 3.26–3.35 (m, 4H, 2 × O–CH_2), 4.14 (q, J = 7.0 Hz, 2H, CH_2), 4.25 (t, J = 7.1 Hz, 2H, N–CH_2), 7.17–7.30 (m, 2H, Ar–H), 7.40–7.69 (m, 5H, Ar–H), 7.76–7.83 (m, 1H, Ar–H) 7.88–7.95 (m, 2H, Ar–H), 8.19 (s, 1H, CH=C), Anal. Calcd for $C_{26}H_{28}N_2O_4$: C, 72.20; H, 6.53; N, 6.48. Found: C, 71.85; H, 6.90; N, 6.35.

*2.8. Compound **48a**–**d** biological activity evaluation*

Biological activity of aminoalkylindoles was evaluated in terms of percentage inhibition and K_i. In both cases, competitive binding assays were performed using membranes from HEK-293 cells transfected with the human recombinant CB_1 receptor (B_{max} = 2.5 pmol/mg protein) and human recombinant CB_2 receptor (B_{max} = 4.7 pmol/mg protein). Receptors were incubated with [^{3}H]-CP-55,940 (0.14 nM/kd = 0.18 nM and 0.084 nM/kd = 0.31 nM respectively for CB_1 and CB_2 receptor) as the high affinity ligand and displaced with 10 μM **WIN 55212-2** as the heterologous competitor for non specific binding (K_i values 9.2 nM and 2.1 nM respectively for CB_1 and CB_2 receptor). All compounds were tested following the procedure described by the manufacturer (Perkin Elmer, Italia). Displacement curves were generated by incubating drugs with **[^{3}H]-CP-55,940** for 90 min at 30 °C. K_i values were calculated by applying the Cheng–Prusoff equation to the IC_{50} values (obtained by GraphPad) for the displacement of the bound radioligand by increasing concentrations of the test compound.

3. Results and discussion

3.1. Human CB2 receptor homology modeling

Since most of the key residues characteristic of GPCRs are conserved in CB2 receptor, a *h*CB2 receptor homology model has

```
pro_Align: pairwise percentage residue identity


  Chains    1    2    3    4
1:P34972       24.6 16.3 20.1
2:2RH1.A  18.9       16.1 17.2
3:3EML.A  20.3 26.1       16.0
4:1F88.A  18.9 21.0 12.1
```

Fig. 2. Pairwise percentage residues identity values calculated evaluated between the four GPCRs.

been generated, starting from the X-ray structures of human β_2 adrenoreceptor (PDB code: 2RH1), human A2A adenosine receptor (PDB code: 3EML) and rhodopsin bovine (PDB: 1F88), as GPCR templates.

The alignment of the CB2 (P34972) fasta sequence on the X-ray coordinates of human β_2 adrenoreceptor [23], human A2A adenosine receptor [24] and rhodopsin bovine [25] was performed on the basis of the Blosum62 matrix (MOE software). The reliability of the four GPCRs alignment can be verified by high values of the pairwise percentage residue identity (PPRI) reported in Fig. 2.

As concern the alignment of the *h*CB2 (P34972) amino acidic sequence on the X-ray coordinates of 2RH1, 3EML and 1F88, the higher PPRI values were the one towards 2RH1 (24.6) and towards 1F88 (20.1), in comparison with that on 3EML (16.3). Thus, the *h*CB2 model was derived by means of the X-ray coordinates of 2RH1 (used as template for *h*CB2 sequence residues 29–227 and 237–316) and 1F88 (used as template for *h*CB2 sequence residues 228–236), aligned together on the basis of the GPCRs conserved residues. The *h*CB2 fragments corresponding to the sequence residues 1–28 and 317–360 were not taken into account, since they are not involved in the agonist–receptor interactions.

As shown in Fig. 3, the following CB2 residues are conserved among the three GPCRs: (*i*) L42, N51 and L64 residues in TM1, (*ii*) Y70, L76, A79, D80, L82 in TM2, (*iii*) L124, A128, the (E/D)RY motif (130–133) in TM3, (*iv*) the A150, W158 and W172 residues in TM4, (*v*) L213 in TM5, (*vi*) the CWXP motif (257-260 amino acids) in TM6, (*vii*) the NPXIY sequence (295–299 residues) and R307 in TM7. In addition, between the target protein and the β_2 adrenoreceptor (which is the most similar template to the *h*CB2 receptor sequence) the following residues are also conserved : (*i*) the L45, V52, V54 and I58 residues in TM1, (*ii*) F72, I73, S75 and A77 in TM2, (*iii*) F106, V113, T118, A119 and S120 in TM3, (*iv*) V152, S161, L163, S165 and L167 in TM4, (*v*) S193, F197 and L201 in TM5, (*vi*) K245, T246, L247 and G220 in TM6, (*vii*) N291, S292 and R302 in TM7.

3.2. Molecular docking of ***WIN-55,212-2***

The obtained CB2 receptor model has been employed to perform a docking procedure on **WIN-55,212-2** (CB2 agonist commonly used in binding experiments) in order to analyse the putative CB2 receptor agonist binding site. In agreement with site-directed mutagenesis data and with the computational results available in literature [31], the agonist selected docking pose occupies a lipophilic pocket delimited by TM3, TM5 and TM6.

In detail (Fig. 4), the oxygen atom of the morpholinic group displays a H-bond interaction with the S112 side chain while the oxygen at the position 7 of the indole moiety shows a H-bond with the N188 backbone. The 1-naphthyl substituent establishes Van der Waals interactions and π–π stacking with W194, L196, F197, I198 and L262.

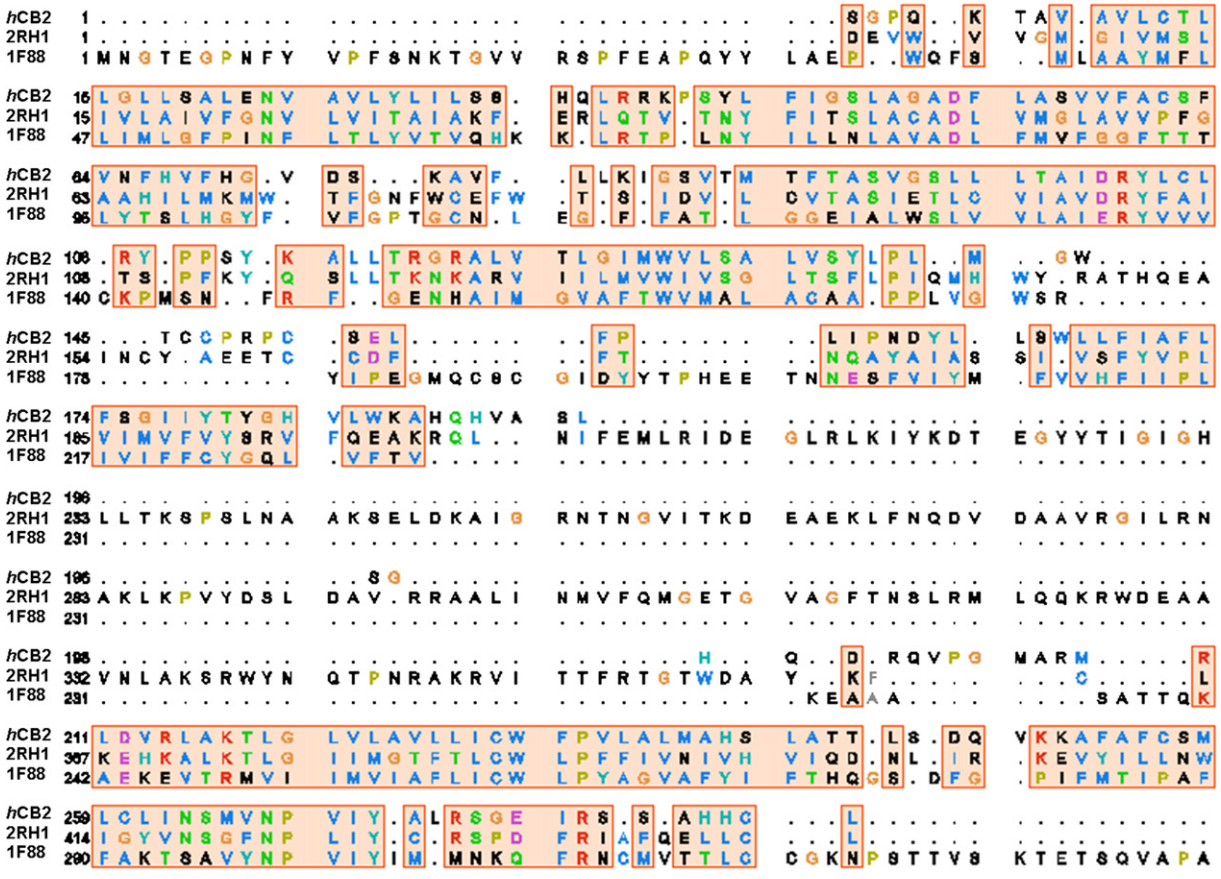

Fig. 3. Sequence alignment of the human CB2 receptor on the basis of the human β_2 adrenoreceptor (2RH1) and the bovine rhodopsin (1F88) coordinates.

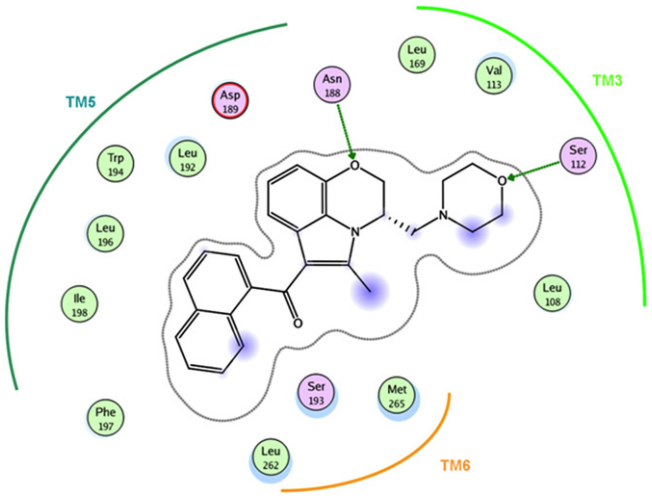

Fig. 4. Selected docking pose of **WIN-55,212-2** into the putative CB2 (obtained by site-directed docking procedure, followed by complex refinement) agonist binding site. H-bond interactions are depicted in green. Residues involved in hydrophobic contacts are labelled. (For interpretation of the references to colour in this figure legend, the reader is referred to the web version of this article.)

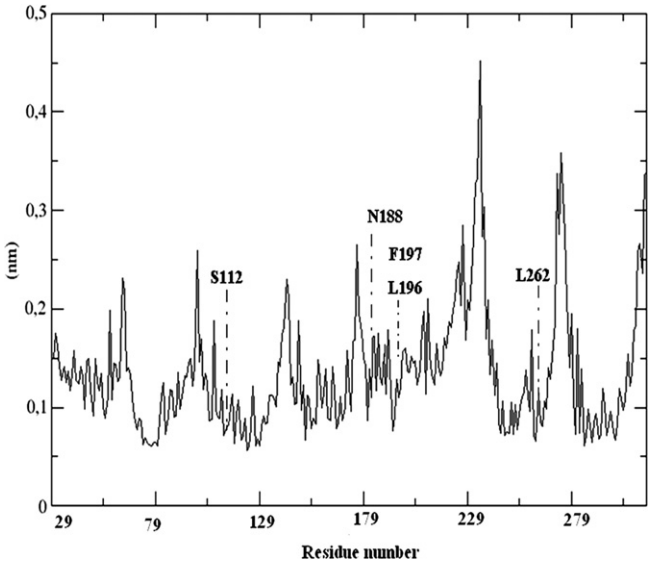

Fig. 5. Graphic of RMS fluctuation of residues in *h*CB2 during the MD simulation (excluding the first 5 ns of equilibration). Residues involved in interactions with the ligand **WIN-55,212-2** are indicated and labelled.

The derived *h*CB2/agonist complex model has been refined by molecular dynamic simulations.

3.3. Molecular dynamic simulations

In order to analyse how the motion of the protein (especially of the side chains in the binding pocket) can influence the binding of the ligand, molecular dynamic (MD) simulations in explicit POPC membrane at physiological temperature (310 K) were performed on the complex between *h*CB2 and agonist **WIN-55,212-2** starting from the conformation obtained by docking simulations. The final trajectory of the complex was energetically stable, with average temperature and pressure close to values of 310 K and 1 bar. The RMSD analysis confirms that the complex reaches an equilibrium after about 5 ns of simulation (see Supplementary Material).

The analysis of root mean square fluctuations (RMSF) can be used as a reference to evaluate motility of the residues of the protein. Here we found that the main fluctuations (>0.2 nm) are present on residues belonging to mobile loops of the protein and on the N-and C-terminal part of the protein, far from the ligand binding pocket. Notably, residues that were found to interact with the agonist in docking simulations, are among the most stable residues of the protein (RMSF < 0.15 nm) (Fig. 5). Also, the ligand shows only limited fluctuations (<0.1 nm) during the simulation. This is crucial, because several important interactions between the protein and the ligand are made *via* H-bonds, and the strength of this kind of bond is determined by the geometry of the interaction, which is strongly affected by mobility of the interactors. In this case, the fluctuations are very low, and it is possible to hypothesize that the interactions between protein and ligand are very stable during the time.

To support this hypothesis, we analyzed the presence and persistence of H-bonds between **WIN- 55,212-2** and *h*CB2 using Gromacs tools. We detected the presence of a maximum of 3 H-bonds with an average number of H-bonds per frame equal to 1.28.

The residues mainly involved in these bonds are S112, which interacts with the oxygen of the morpholine ring moiety (atom OBE) and S285, bound to the methyl morpholine ring moiety (atom NAB). We also measured the variation of the distances between these atoms during the simulation (Fig. 6), and found that the distances between S112 and atom OBE and between S285 and NAB are stable around 3 Å from 6 to 20 ns. Instead, from MD data, the H-bond between N188 residue with the oxygen of the naphthyl methanone moiety (atom NAB) seems to be less stable since the distance between the donor and the acceptor atom is variable between 2.5 and 11.5 A during the simulation.

In order to analyse the variability among different frames of the simulation, we carried out a cluster analysis on the trajectory. The calculation using a cut-off of 0.1 nm for the RMSD after partial least-square fit, calculated on the structure of the protein, produced only a single cluster for the whole trajectory. The same result was obtained using as a reference the structure of the ligand.

These results indicate the high similarity between the structures in the simulation and suggest that no important differences are present among the several structures in terms of ligand motility, as it was also suggested by the low RMSF value.

Finally, we compared the representative structure of the complex obtained from the trajectory with the one derived from docking simulation.

The comparison between the docking and molecular dynamics studies shows a different binding mode of the agonist in the putative pocket. The hydrogen bonded pattern is conserved for residues S112 and N188 in both simulations; molecular dynamics shows an additional hydrogen bond involving the S285 (Fig. 7).

Therefore, the molecular portrait obtained by MD simulation is that of a protein in which the ligand is bound with a high conformational stability, and in which H-bonds and hydrophobic interactions keep the molecule strictly associated to the protein, confirming the hypotheses made on the basis of docking experiments.

The final model backbone conformation was inspected by Ramachandran plot, showing absence of outliers among the residues belonging to the putative binding site (see Fig. S1 in the supplementary data). As depicted in Fig. 8, the derived *h*CB2 model was superimposed to the coordinates of the human β_2 adrenoreceptor, which is the template showing the higher similarity to the target protein [compare the *h*CB2 PPRI value towards 2RH1 (24.6) with those on 1F88 (20.1)], displaying a quite positive root mean square deviation value (RMSD = 1.113 Å, calculated on the carbon atom alignment).

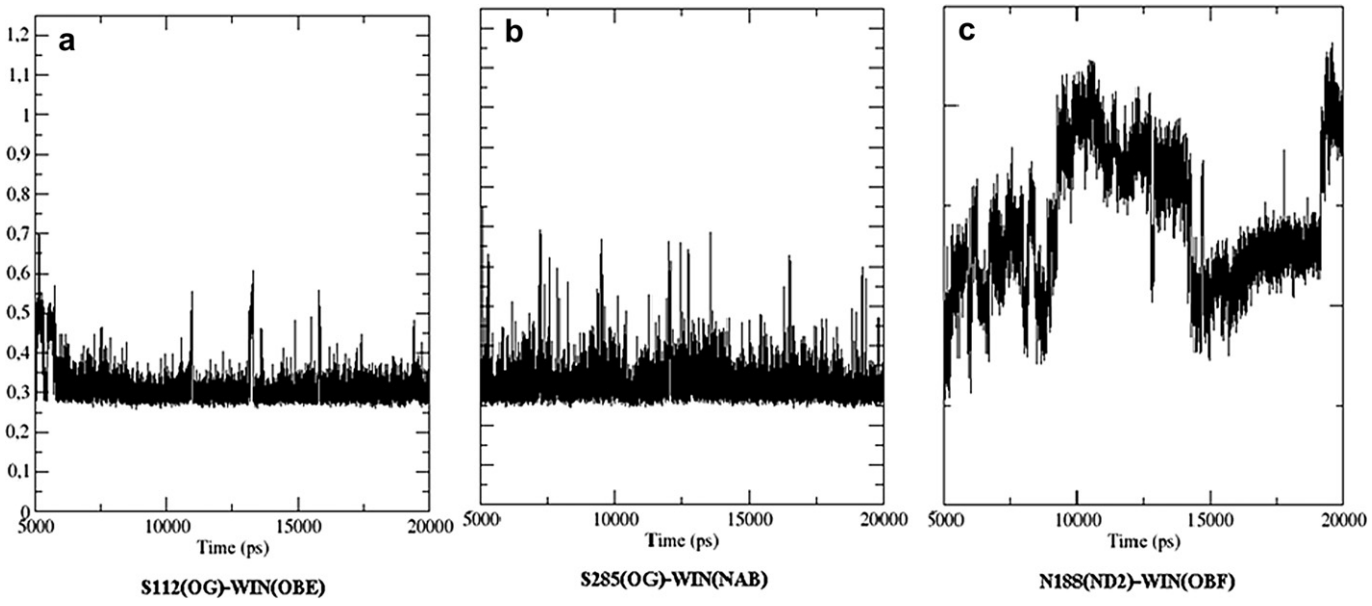

Fig. 6. Variation of distances of heavy atoms (donor and acceptor) involved in H-bonds between *h*CB2 and **WIN-55,212-2** (excluding the first 5 ns of equilibration). Distance between side chain oxygen of S112 and morpholine ring moiety (atom OBE) (a); distance between side chain oxygen of S285 and the methyl morpholine ring moiety (atom NAB) (b); distance between amide nitrogen of N188 and oxygen of the naphthyl methanone moiety (atom NAB) (c).

As shown in Fig. 9, the agonist **WIN-55,212** is surrounded by the following conserved residues: (*i*) V113 in TM3, (*ii*) S193 and F197 in TM5, (*iii*) W258 in TM6.

Notably, the F197 and W258 side chain are the only conserved residues which resulted to be rotated, in comparison with those of the β_2 adrenoreceptor, being more in proximity and slightly far from the agonist, respectively. Consequently, according to our studies, the geometry of the derived *h*CB2 model binding pocket seems to be particularly affected by the establishment of hydrophobic contacts, such as those with F197.

3.4. Molecular docking of compounds **1**–**46**

In order to verify if the protein model built (and the docking protocol previously applied) could be employed as a reliable tool for virtual screening procedures (by explaining why a compound could be a more or less active *h*CB2agonist), we performed docking simulations on a series of known potent *h*CB2 agonists.

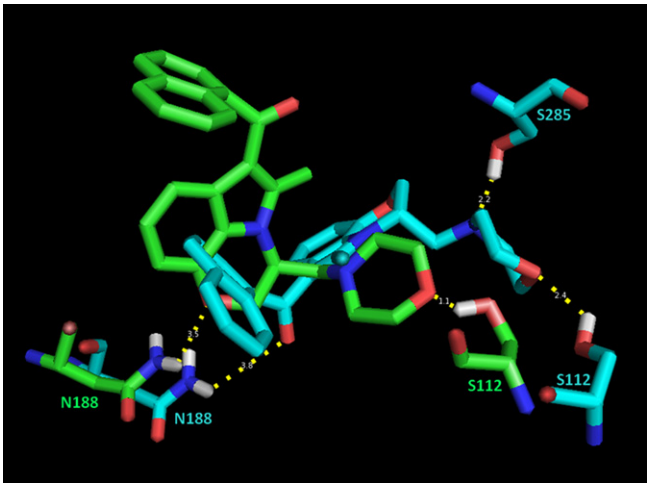

Fig. 7. The **WIN-55,212-2** poses (green) and (cyan) obtained by docking and molecular dynamics simulations respectively. Only residues involved in the hydrogen bond-interactions are depicted in stick and labelled. (For interpretation of the references to colour in this figure legend, the reader is referred to the web version of this article).

Thus, the derived **WIN-55,212-2**/receptor complex has been used as starting point for the automatic docking simulation on a series of indol-3-yl-tetramethylcyclopropyl ketone derivatives.

According to our calculations all the indol-3-yl-tetramethylcyclopropyl ketone derivatives display a H-bond interaction with S112 side chain by the oxygen atom of the carbonyl group and share the following Van der Waals contacts between: (*i*) the R1 substituent and L108, V113, L169, (*ii*) the tetramethylcyclopropyl ketone portion and the F87, F117 and C288 side chain, (*iii*) the agonist indole moiety and L108, and M265.

More in details, as shown in Fig. 10, **17** (the most active compound of the series) is engaged in two additional H-bond contacts between the methoxy group at the indole position 7 and the N188 side chain, and between the pyrane oxygen atom and the T114 nitrogen atom.

On the contrary, compound **13**, bearing a hydroxyl group at the indole position 7, displays H-bond contact between the R7 substituent and the P184 carbonyl oxygen atom, while any interactions concerning the pyrane oxygen atom are missing.

Similarly, compounds **14**, **15**, **16**, bearing the methoxy group at the indole position 4, 5 and 6, respectively, are also unable to display H-bonds with T114. On the other hand, the compound **14, 15** methoxy groups, and the one of compound **16,** are involved in H-bond interactions with the L182 and the L185 nitrogen atom, respectively.

Accordingly, compound **13** ($pIC_{50} = 8.50$) and compound **14**–**16** ($pIC_{50} = 8.34$–9.29) show lower pIC_{50} values in comparison with that of compound **17** ($pIC_{50} = 9.90$).

Compounds **10** ($pIC_{50} = 8.41$), **11** ($pIC_{50} = 8.72$), **12** ($pIC_{50} = 8.07$), bearing the hydroxyl moiety at the indole position 4, 5 and 6, miss any contacts between the pyrane ring and T114, but compound **10** and **11** seem to be engaged in H-bonds with the S285 side chain, being more potent than compound **12**.

Compound **41** (indole **15** analogue) and compound **42** (indole **16** analogue), bearing an ethyl-morpholine substituent at the indole position 1 (instead of a methyl-pyrane one), are not able to properly interact with the L182 and L185 nitrogen atom, respectively.

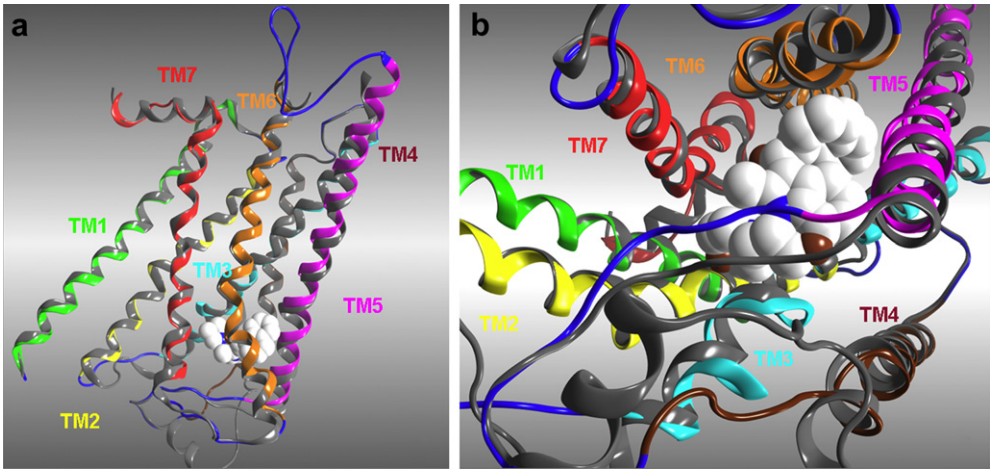

Fig. 8. The superimposition of the final *h*CB2 model on the 2RH1 coordinates is depicted as side-view (a) and as top-view (b). The **WIN-55,212-2** pose is depicted by space filling curve.

In fact, compound **41** misses any H-bond interaction with L182 while, as shown in Fig. 11, **42** displays an H-bond contact with the N188 backbone nitrogen atom.

Accordingly, compounds **41** ($pIC_{50} = 6.63$) and **42** ($pIC_{50} = 8.80$) show lower pIC_{50} values in comparison with those of compound **15** ($pIC_{50} = 8.34$) and compound **16** ($pIC_{50} = 9.29$).

For the indole selected docking poses, scoring function values have been reported in Table S2 (supplementary data).

3.5. CoMFA and CoMSIA analyses

The compound selected docking poses, aligned into the *h*CB2 putative binding site, were submitted to 3D-QSAR studies.

CoMFA and CoMSIA analyses were performed dividing compounds **1**–**46** into a training set (**2**–**14, 16**–**23, 25**–**31, 33, 34, 36, 38, 40, 42, 43, 45, 46**) for model generation and into a test set (**1, 15, 24, 32, 35, 37, 39, 41, 44**) for model validation. CoMFA and CoMSIA studies were developed using, respectively, CoMFA steric and electrostatic fields and CoMSIA steric, electrostatic, hydrophobic, H-bond acceptor and H-bond donor properties, as independent variables, and the ligand pK_i as dependent variable.

The final CoMFA model was generated employing non-cross-validated PLS analysis with the optimum number of components (ONC = 6) to give a non-cross validated r^2 (r^2_{ncv}) = 0.94, a test set r^2 (r^2_{pred}) = 0.71, Standard Error of Estimate (SEE) = 0.245, steric contribution = 0.461 and electrostatic contribution = 0.539. The model reliability thus generated was supported by bootstrapping results. All statistical parameters supporting CoMFA model are reported in Table 3.

The final CoMSIA model consisting of steric, electrostatic, hydrophobic, H-bond acceptor and H-bond donor fields with a $r^2_{ncv} = 0.96$, $r^2_{pred} = 0.78$, SEE = 0.193, steric contribution = 0.110, electrostatic contribution = 0.231, hydrophobic contribution = 0.159, H-bond acceptor contribution = 0.241 and H-bond donor contribution = 0.259 was derived. All statistical parameters supporting CoMSIA model are reported in Table 3.

Experimental and predicted binding affinities values for the training set and test set are reported in Table 4, while distribution of experimental and predicted pK_i values for training set according to the final CoMFA and CoMSIA models are represented in Fig. S3 (supplementary data).

On the basis that CoMFA and CoMSIA field effects on the target properties can be viewed as 3D coefficient contour plots, identifying important regions where any change in these fields may affect the compound affinity, they could be helpful to optimize indol-3-yl-tetramethylcyclopropyl ketones as CB2 agonists. The 3D-QSAR

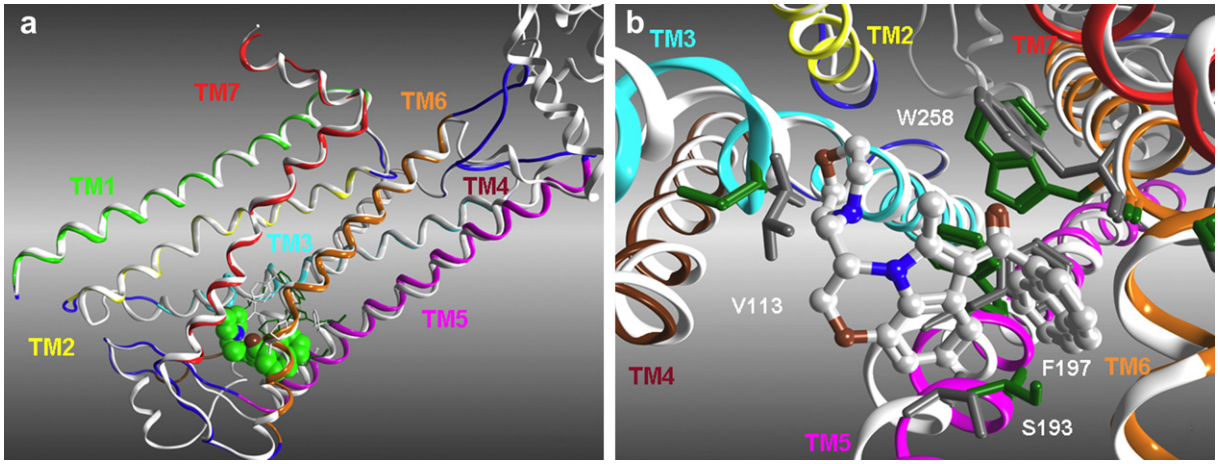

Fig. 9. The superimposition of the final *h*CB2 model on the 2RH1 coordinates is depicted: (a) the two proteins are shown as side-view and the **WIN-55,212-2** pose is depicted by space filling curve. (b) the two proteins are shown as top-view and the **WIN-55,212-2** pose is depicted by ball and stick. The conserved residues located 5 Å from the agonist are shown and labelled.

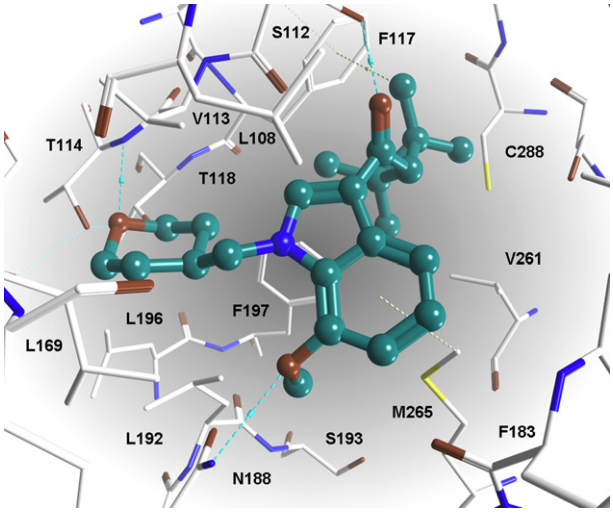

Fig. 10. The compound **17** selected docking into the *h*CB2 putative binding site is depicted. The agonist is reported in ball and stick, C atom in dark green. Residues located 5 Å from the agonist are shown and labelled. H-bond are coloured in cyano. (For interpretation of the references to colour in this figure legend, the reader is referred to the web version of this article.)

analysis maps are described and discussed in the following sections.

3.5.1. CoMFA steric and electrostatic regions

As shown in Fig. 12a (for simplicity, only the structure of compound **17**, showing the highest pK_i value in the dataset, is depicted and used as a model) the steric contour map predicts favourable interaction polyhedra (green) for positions 4, 6 and 7 of the indole moiety, around the tetramethylcyclopropyl group and in proximity of the pyrane ring. The introduction of bulky group around position 5 of the indole scaffold is disfavoured (yellow). The reliability of the steric map calculations is verified by the higher pKi value of **17** (R7 = OCH_3, pK_i = 9.90) in comparison with that of **13** (R7 = OH, pK_i = 8.50) and by the higher affinity of **6** (R6 = bromo, pK_i = 9.19), **16** (R6 = OCH_3, pK_i = 9.29), **35** (R5 = OH, R6 = OCH_3,

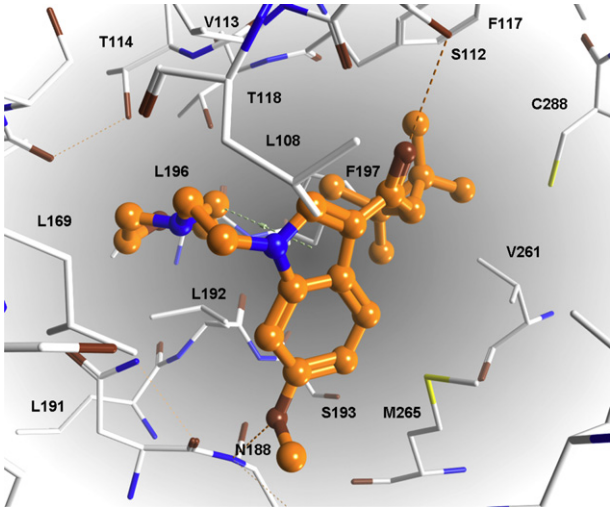

Fig. 11. The compound **41** selected docking into the *h*CB2 putative binding site is depicted. The agonist is reported in ball and stick, C atom in orange. Residues located 5 Å from the agonist are shown and labelled. H-bond are coloured in red. (For interpretation of the references to colour in this figure legend, the reader is referred to the web version of this article.)

Table 3
Summary of CoMFA and CoMSIA results.

	CoMFA Model	CoMSIA Model
No. compounds	37	37
Optimal number of components (ONC)	6	6
Leave one out r^2 (r^2_{loo})	0.562	0.602
Cross-validated r^2 (r^2_{cv})	0.678	0.713
Std. error of estimate (SEE)	0.245	0.193
Non cross-validated r^2 (r^2_{ncv})	0.94	0.96
F value	76.178	125.223
Steric contribution	0.461	0.110
Electrostatic contribution	0.539	0.231
Hydrophobic contribution	–	0.159
H-bond acceptor contribution	–	0.241
H-bond donor contribution	–	0.259
Bootstrap r^2 (r^2_{boot})	0.97	0.98
Standard error of estimate r^2_{boot} (SEE r^2_{boot})	0.169	0.149
Test set r^2 (r^2_{pred})	0.71	0.78

Table 4
Experimental and predicted pK_i values of compounds **1**–**46**.

Compound		CoMFA Model		CoMSIA Model	
	Exp. pK_i	Pred. pK_i	Pred. pK_i	Pred. pK_i	Residual
1[a]	8.31	8.41	−0.10	7.93	0.38
2	8.80	8.61	0.19	8.57	0.23
3	8.52	8.46	0.06	8.46	0.06
4	8.18	8.32	−0.14	8.60	−0.42
5	8.60	8.52	0.08	8.90	−0.30
6	9.19	8.79	0.40	8.97	0.22
7	9.83	9.28	0.55	9.33	0.50
8	8.46	8.89	−0.43	8.69	−0.23
9	8.53	8.59	−0.06	8.73	−0.20
10	8.41	8.91	−0.49	8.68	−0.27
11	8.72	8.46	0.26	8.87	−0.15
12	8.07	7.81	0.26	7.97	0.10
13	8.50	8.43	0.07	8.50	0.00
14	8.48	8.24	0.24	8.75	−0.27
15[a]	8.34	8.04	0.30	8.63	−0.29
16	9.29	9.67	−0.38	9.31	−0.02
17	9.90	9.86	0.04	9.51	0.39
18	8.03	8.08	−0.04	8.09	−0.06
19	8.90	8.69	0.21	8.62	0.28
20	9.05	9.27	−0.22	9.16	−0.11
21	8.52	8.44	0.08	8.99	−0.47
22	8.03	8.16	−0.13	8.05	−0.02
23	6.58	6.62	−0.04	6.38	0.21
24[a]	7.14	7.37	−0.23	7.59	−0.45
25	7.52	7.73	−0.21	7.46	0.06
26	6.95	7.04	−0.09	7.02	−0.07
27	7.59	7.55	0.04	7.68	−0.09
28	6.62	6.56	0.06	6.47	0.15
29	7.23	7.14	0.09	7.39	−0.16
30	8.30	8.45	−0.15	8.52	−0.22
31	7.21	7.53	−0.32	6.93	0.28
32[a]	8.86	7.81	1.05	8.21	0.65
33	9.39	9.32	0.07	9.41	−0.02
34	8.75	8.81	−0.06	8.84	−0.09
35[a]	9.16	8.77	0.39	8.87	0.30
36	7.67	7.94	−0.27	7.56	0.11
37[a]	8.99	8.36	0.64	8.67	0.33
38	8.36	8.53	−0.17	8.40	−0.04
39[a]	7.04	7.29	−0.25	7.50	−0.46
40	6.96	6.85	0.11	7.20	−0.24
41[a]	6.63	7.09	−0.46	7.15	−0.52
42	8.80	8.72	0.08	8.54	0.26
43	8.53	8.51	0.02	8.39	0.14
44[a]	7.57	7.72	−0.15	7.87	−0.30
45	6.53	6.49	0.04	6.74	−0.21
46	7.49	7.46	0.03	7.33	0.16

[a] Test set compounds.

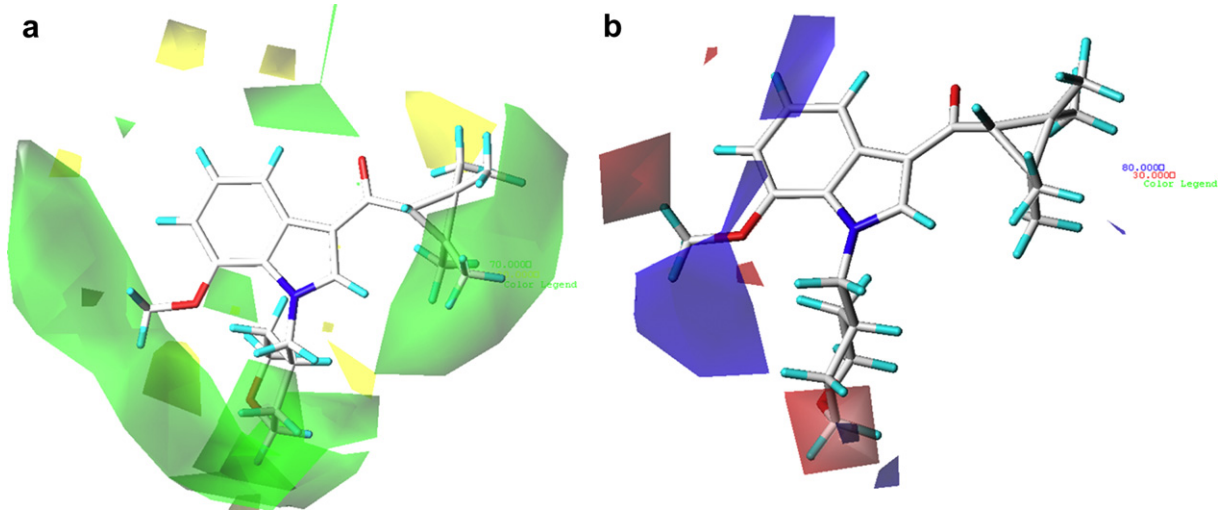

Fig. 12. Contour maps of CoMFA steric regions (green, favoured; yellow, disfavoured) are displayed around compound **17**, depicted in stick mode and coloured by atom type (a). Contour maps of CoMFA electrostatic regions are shown around compound **17**. Blue regions are favourable for more positively charged groups; red regions are favourable for less positively charged groups (b). (For interpretation of the references to colour in this figure legend, the reader is referred to the web version of this article.)

$pK_i = 9.16$) and **42** (R6 = OCH_3, $pK_i = 8.80$) compared to those of **5** (R6 = chloro, $pK_i = 8.60$), **12** (R6 = OH, $pK_i = 8.07$), **36** (R5 = OH, R6 = OH, $pK_i = 7.67$) and **40** (R6 = OH, $pK_i = 6.96$), respectively. Moreover, the results are in agreement with the high binding affinity of **33** (R6 = phenyl, $pK_i = 9.39$), with the higher pK_i of **10** (R4 = OH, $pK_i = 8.41$) and **14** (R4 = OCH_3, $pK_i = 8.48$) compared to that of **18** (R4 = OCH_2Ph, $pK_i = 8.03$), and with the following affinity trends: **2** (R5 = fluoro, $pK_i = 8.80$) > **3** (R5 = chlorine, $pK_i = 8.52$) > **4** (R5 = bromo, pKi = 8.18); **11** (R5 = OH, $pK_i = 8.72$) > **15** (R5 = OCH_3, $pK_i = 8.34$) > **27** (R6 = CH_2OCH_3, $pK_i = 7.59$); **38** (R5 = H, $pK_i = 8.36$) > **39** (R5 = OH, $pK_i = 7.04$) > **41** (R5 = OCH_3, $pK_i = 6.63$). Accordingly, compound **35** (R5 = OH, R6 = OCH_3, $pK_i = 9.16$) shows higher binding affinity value than **34** (R5 = OCH_2Ph, R6 = OCH_3, $pK_i = 8.75$).

According to the electrostatic field contour maps of the CoMFA analysis plotted in Fig. 12b, less positive moieties are predicted to be favoured (red areas) around the pyrane oxygen atom and the indole positions 6 and 7. On the other side, more electropositive substituents are predicted to be beneficial (blue polyhedra) in the vicinity of the indole positions 4 and 5. These results are in agreement with the higher pK_i values of **5** (R6 = chlorine), **6** (R6 = bromo), **9** (R6 = SO_2CH_3), **16** (R6 = OCH_3), **30** (R6 = CN), **32** (R6 = CO_2CH_3) and **33** (R6 = phenyl) ($pK_i = 8.30–9.39$) in comparison with that of **31** (R6 = CH_2NH_2, pKi = 7.21) and are also supported by the evidence of the higher affinity levels of **17** (R7 = OCH_3, $pK_i = 9.90$), **42** (R6 = OCH_3, $pK_i = 8.80$) and **35** (R5 = OH, R6 = OCH_3, $pK_i = 9.16$) in comparison to those of **13** (R7 = OH, $pK_i = 8.50$), **40** (R6 = OH, $pK_i = 6.96$) and **36** (R5 = OH, R6 = OH, $pK_i = 7.67$), respectively. The results are also in accordance with the higher pK_i values of **11** (R5 = OH, $pK_i = 8.72$) and **39** (R5 = OH, $pK_i = 7.04$) compared to those of **15** (R5 = OCH_3, $pK_i = 8.34$) and **41** (R5 = OCH_3, $pK_i = 6.63$), respectively, and with the following affinity trend: **2** (R5 = fluoro, $pK_i = 8.80$) > **3** (R5 = chloro, $pK_i = 8.52$) > **4** (R5 = bromo, $pK_i = 8.18$). Finally, compounds **11** (R5 = OH, $pK_i = 8.72$) and **39** (R5 = OH, $pK_i = 7.04$) display higher binding affinity than **15** (R5 = OCH_3, $pK_i = 8.34$) and **41** (R5 = OCH_3, $pK_i = 6.63$), respectively.

The CoMSIA steric and electrostatic regions are in agreement with the CoMFA steric and electrostatic areas.

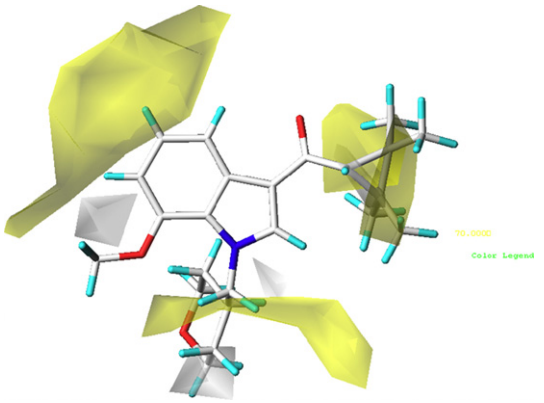

Fig. 13. Contour maps of CoMSIA hydrophobic regions (yellow, favoured; white, disfavoured) are shown around compounds **17**, shown in stick mode and coloured by atom type. (For interpretation of the references to colour in this figure legend, the reader is referred to the web version of this article.)

3.5.2. CoMSIA hydrophobic, H-bond acceptor and H-bond donor regions

The calculated CoMSIA hydrophobic contours (Fig. 13) predict favourable hydrophobic substituents (yellow areas) around the tetramethylcyclopropil group, the positions 4 and 5 of the indole moiety and in proximity of positions 5 and 6 of the pyrane ring. On the contrary, lipophilic substituents around the 6 and 7 positions of indole moiety result to be disfavoured (white polyhedra). The reliability of the hydrophobic map calculations is verified by higher affinity of **19** (R5 = OCH_2Ph, $pK_i = 8.90$), **24** (R5 = $O(CH_2)_4Br$, $pK_i = 7.14$), and **27** (R5 = CH_2OCH_3, $pK_i = 7.59$) compared to those of **15** (R5 = OCH_3, $pK_i = 8.34$), **23** (R5 = $O(CH_2)_4OH$, $pK_i = 6.58$), and **26** (R5 = CH_2OH, $pK_i = 6.95$), respectively. These results are in agreement with the difference in pKi levels between: (*i*) **7** (R6 = CH_3, $pK_i = 9.83$) and **8** (R6 = CF_3, $pK_i = 8.46$); (*ii*) **16** (R6 = OCH_3, $pK_i = 9.29$) and **20** (R6 = OCH_2Ph, $pK_i = 9.05$); (*iii*) **32** (R6 = CO_2CH_3, $pK_i = 8.86$) and **9** (R6 = SO_2CH_3, $pK_i = 8.53$); (*iv*) **42** (R6 = OCH_3, $pK_i = 8.80$) and **43** (R6 = OCH_2Ph, $pK_i = 8.53$); (*v*) **17** (R7 = OCH_3, $pK_i = 9.90$) and **21** (R7 = OCH_2Ph, $pK_i = 8.52$).

To take into account the role of H-bond acceptor and H-bond donor groups for the affinity towards the human CB2 receptor, the corresponding CoMSIA contours were calculated. As shown in Fig. 14a, H-bond acceptor groups are predicted to be favoured (magenta regions) around the oxygen atom of pyrane ring, the

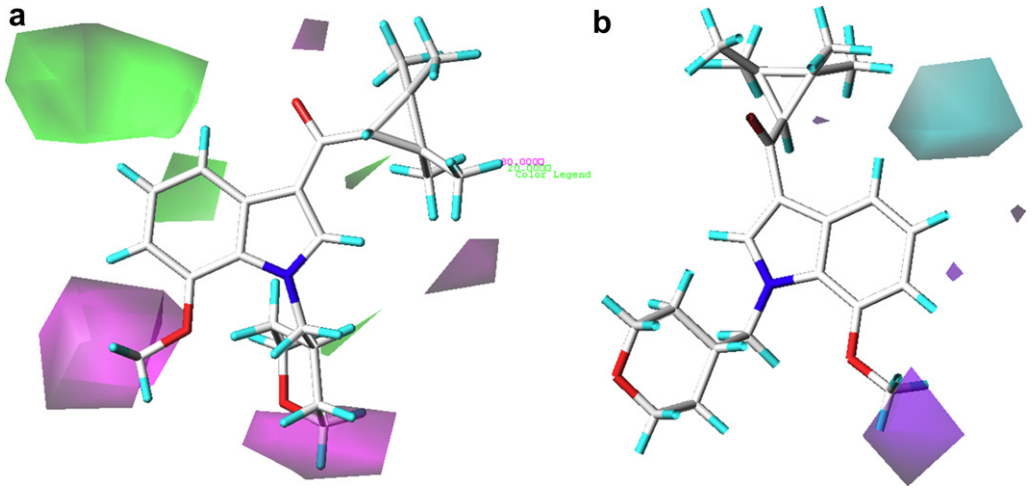

Fig. 14. CoMSIA hydrogen bond acceptor polyhedra are shown around compounds **17**, depicted in stick mode and coloured by atom type. H-bond acceptor groups: magenta, favoured; green, disfavoured (a). CoMSIA hydrogen bond donor polyhedra are shown around compounds **17**, depicted in stick mode and coloured by atom type. H-bond donor groups: purple, disfavoured; cyan, favoured (b). (For interpretation of the references to colour in this figure legend, the reader is referred to the web version of this article.)

oxygen atom of carbonyl function and in proximity of the indole position 7. Besides, H-bond donors (Fig. 14b) are predicted to be beneficial (cyan areas) in the vicinity of the indole position 4, while the introduction of a H-donor group seems to be disfavoured (purple) in a small area close to the R7 methoxy group in compound **17**. The reliability of these calculations is verified by the higher affinity of **46** (R4 = NH_2, pKi = 7.49) in comparison to that of **45** (R4 = NO_2, pKi = 6.53).

3.5.3. *A comparison between the CoMFA and CoMSIA analyses and the hCB2/**17** docking model*

In order to verify the reliability of the 3D-QSAR model, CoMFA and CoMSIA maps have been compared with the docking analysis results. For simplicity, in Figs. S4–S7 (supplementary data) we have reported only the CoMFA steric, electrostatic and the CoMSIA hydrophobic and the H-bond acceptor maps, superimposed to the docking model of compound **17** into the putative receptor binding site.

The CoMFA steric model proves to match with the *h*CB2 putative binding site 3D topology, suggesting bulky substitution in proximity of three deep receptor pockets (Fig. S4). The first cavity (P1), including F87, S112, F117, L182 and C288, surrounds the tetramethylcyclopropyl group, while the second pocket (P2, delimited by L108, V113, T114, S165 and L169) is occupied by the substituent at the indole position 1. Finally, the substituents located at the indole position 6 and 7 are oriented towards a third receptor pocket (P3), including residues N188, L192, L196 and F197. As shown in Fig. S5, the CoMFA electrostatic map highlights the importance of electronegative groups at the indole position 1 and 7, which could be involved in H-bond interactions with the key residues T114 and N188. The CoMSIA hydrophobic (Fig. S6) map points out the beneficial presence of hydrophobic substituents at the following positions: (*i*) at the indole position 5, establishing hydrophobic contacts with M265, C288, (*ii*) in proximity of the tetramethylcyclopropyl group, enhancing interactions with F87, L182 and L289, (*iii*) and around the methylene located between the indole position 1 and the pyrane ring, being probably involved in contacts with the residues L108 and L192. The CoMSIA H-bond donor and H-bond acceptor maps (Fig. S7) confirm the importance of the formation of the hydrogen bond between the indole derivative carbonyl group and S112, and between the pyrane ring oxygen atom and N188. Furthermore, the introduction of H-donor groups onto the indole position 4 can allow the establishment of H-bond contacts with S285.

The information obtained by the 3D-QSAR contour maps and the molecular docking studies provide useful suggestions for the synthesis of new indol-3-yl-tetramethylcyclopropyl ketone derivatives with possible improved potency. In detail, a 2- methyl, 6-methyl or 2,6-dimethylpyrane ring would seem particularly favourable as substituent R1, detecting hydrophobic contacts with L108, V113, T114, and L169. Regarding the indole moiety, an alkyl amine group at position 4 could enhance the ligand potency by H-bond interactions with S285 (when R7 is a methoxy group, being H-bonded to N188). On the other hand (when R4 is a hydroxyl group,

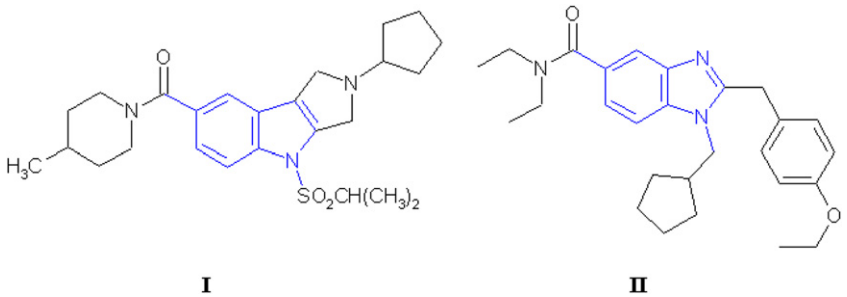

I **II**

Fig. 15. Chemical structure of selective CB2 agonists **I** and **II** (showing the highest pKi values in the 1,2,3,4-tetrahydropyrrolo[3,4-*b*]indole series and in the benzimidazole series, respectively). The common 1,5-disubstituted-indole or −benzimidazole scaffold is depicted in blue. (For interpretation of the references to colour in this figure legend, the reader is referred to the web version of this article.)

Table 5
Binding affinities of compounds **48a**–**48d** towards hCB$_1$ and hCB$_2$ receptors.

Compound	CoMFA Model mmmmodelModel	CoMSIA Model
	Pred. pK$_i$	Pred. pK$_i$
48a	8.68	8.43
48b	7.01	6.34
48c	8.32	8.27
48d	6.83	6.28

representative compounds **I** and **II** are depicted) have shown high binding affinity toward CB2 receptor and good selectivity over CB1 receptor.

Thus, in order to identify the key structural features impacting the binding affinity, a computational study of 3D-QSAR was performed. Initially, the two classes of selective CB2 agonists were studied separately (one CoMFA and one CoMSIA model for each series was derived), subsequently, all compounds together were

Table 6
Binding affinities of compounds **48a**–**48d** towards hCB$_1$ and hCB$_2$ receptors.

Compd	Displacement% on CB1[a]	IC$_{50}$ on CB1 μM	K$_i$ on CB1 μM	Displacement% on CB2[b]	IC$_{50}$ on CB2 μM	K$_i$ on CB2 μM	Exp. pK$_i$ on CB2
48a	at 10 μM (83.00)		163.4	at 10 μM (101.00)		0.0075	8.12
48b	at 10 μM (25.08)	>10	>10	at 10 μM (70.75)	5.48	1.39	5.86
48c	at 1 μM (85.01)	0.155	0.062	at 1 μM (95.93)	0.0401	0.0102	7.99
48d	at 10 μM (43.22)	>10	>10	at 10 μM (66.04)	6.22	1.58	5.80

[a] Data reported as percent of displacement of [^{3}H]-CP 55,940 (0.5 nM) from hCB$_1$ receptor, at an inhibitor concentration of 10 or 1 μM.
[b] Data reported as percent of displacement of [^{3}H]-**WIN 55,212-2** (0.8 nM) from hCB$_2$ receptor, at an inhibitor concentration of 10 or 1 μM.

being H-bonded to S285), an aminomethyl- or aminomethyl group (NH2CH2- or NH2CH2CH2-) could be introduced at the indole position 7, being engaged in H-bond with N188. In addition, the indole position 6 could be exploited to establish hydrophobic contacts with L196 and F197 by introducing a small alkyl group.

3.6. Newly synthesized compounds ***48a–d***

On the basis of the 3D-QSAR analyses previously discussed, several favourable structural modifications on the indole moiety have been identified. Among them, the introduction of H-bond acceptor groups around the indole position 1 and 3 (see Fig. 14a) emerged to be particularly interesting. In order to verify the reliability of these results, we compared the CoMSIA maps obtained on compounds **1**–**47** with those derived from CoMFA and CoMSIA studies, already performed by us, on other two series of CB2 agonists, structurally related to indole derivatives [56]. Briefly, novel classes of CB2 agonists based on 1,2,3,4-tetrahydropyrrolo [3,4-*b*]indole and benzimidazole scaffolds [57,58] (in Fig. 15, aligned (on the basis of the common scaffold depicted in blue in Fig. 15), and the final CoMFA and CoMSIA models were calculated.

As concern the indole positions 1 and 3 discussed above, 3D-QSAR studies performed on 1,2,3,4-tetrahydropyrrolo[3,4-*b*]indole and benzimidazole derivatives point out that the following key features could enhance the ligand hCB2 agonist activity: *(i)* bulky substituents bearing electronegative (and H-bond acceptor) groups at the indole position 1 (see Fig. 15), *(ii)* electronegative (and H-bond acceptor) groups located between the indole position 3 and a bulky hydrophobic substituent (see Fig. 15).

Accordingly, four aminoalkylindoles have been designed and synthesized, bearing an aminoalkyl group and a vinyl moiety (disubstituted by polar groups) at the indole position 1 and 3, respectively. For these compounds, the predicted pK$_i$ values (by means of the CoMSIA model calculated on indoles **1**–**47**), have been listed in Table 5.

As reported in Table 6, compounds **48a** and **48c** show high K$_i$ values towards the human CB2 receptor, within a nanomolar range while compounds **48b** and **48d** show binding affinities in the micromolar range. Notably, compound **48a** proves to be a CB2 selective ligand.

The MD CB2/agonist complex previously discussed has been employed to perform molecular docking studies on indoles **48a**–**48d**, in order to rationalize the biological data and to investigate their binding mode within the molecular target. The most interesting compound, **48a** (Fig. 16), displays H-bond contacts between the sulphonyl and the N188 side chain, and between the pyperidine protonated nitrogen atom and the key residue S112. The indole moiety is engaged in π–π with F117 and F197, and in Van der Waals contacts with V261. The Y cyano and phenyl group are properly oriented towards residues T114 and T118, and towards L182 and L185, respectively.

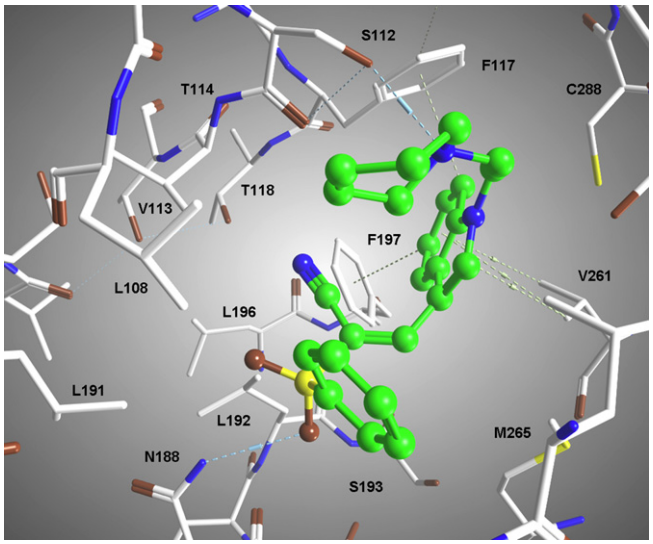

Fig. 16. Compound **48a** (green) selected docking pose into the MD hCB2/**WIN-55,212-2** complex. Only residues involved in ligand/receptor interactions are depicted in stick and labelled. H-bond are depicted in cyano. (For interpretation of the references to colour in this figure legend, the reader is referred to the web version of this article.)

4. Conclusions

In this work, with the aim of gaining a better understanding of the agonist-CB2 receptor interactions, a theoretical model of the human CB2 receptor (hCB2) developed by homology modeling and molecular dynamic techniques has been discussed. The model and docking protocol reliability has been verified by docking studies on a series of potent CB2 agonists (indol-3-yl-tetramethylcyclopropyl ketone derivatives). Successively, the docking-based CoMFA and CoMSIA analyses, performed on the same series of compounds, allowed us to derive more complete guidelines for the design of

new analogues with improved potency so as to synthesize new indoles showing high CB2 affinity.

Acknowledgements

This work was financially supported by the University of Genova, MIUR FIRB ITALBIONET (RBPR05ZK2Z and RBIN064YAT_003), flagship InterOmics. Prof. Stefano Moro, Dr. Marco Fanton and Dr. Giuseppe Marson are gratefully acknowledged. E.C. was financially supported by a post-doc fellowship, Area Chimica, University of Genova.

Appendix. Supplementary material

Supplementary data associated with this article can be found, in the online version, at doi:10.1016/j.ejmech.2011.07.023.

References

[1] S.L. Palmer, G.A. Thakur, A. Makriyannis, Cannabinergic ligands, Chem. Phys. Lipids 121 (2002) 3–19.
[2] A.C. Howlett, F. Barth, T.I. Bonner, G. Cabral, P. Casellas, W.A. Devane, C.C. Felder, M. Herkenham, K. Mackie, B.R. Martin, R. Mechoulam, R.G. Pertwee, International Union of Pharmacology. XXVII. Classification of cannabinoid receptors, Pharmacol. Rev. 54 (2002) 161–202.
[3] R.G. Pertwee, Cannabinoid receptors and pain, Prog. Neurobiol. 63 (2001) 569–611.
[4] P. Goya, N. Jagerovic, L. Hernandez-Folgado, M.I. Martin, Cannabinoids and neuropathic pain, Mini Rev. Med. Chem. 3 (2003) 765–772.
[5] A. Calignano, G. La Rana, D. Piomelli, Antinociceptive activity of the endogenous fatty acid amide, palmitylethanolamide, Eur. J. Pharmacol. 419 (2001) 191–198.
[6] V. Di Marzo, C.S. Breivogel, Q. Tao, D.T. Bridgen, R.K. Razdan, A.M. Zimmer, B.R. Martin, Levels, metabolism, and pharmacological activity of anandamide in CB(1) cannabinoid receptor knockout mice: evidence for non-CB(1), non-CB(2) receptor-mediated actions of anandamide in mouse brain, Neurochemistry 75 (2000) 2434–2444.http://www.ncbi.nlm.nih.gov/pubmed/11080195.
[7] N. Hájos, C. Ledent, T.F. Freund, Cannabinoids inhibit hippocampal GABAergic transmission and network oscillations, Neuroscience 12 (2000) 3239–3249.
[8] G.T. Whiteside, G.P. Lee, K.J. Valenzano, The role of the cannabinoid CB2 receptor in pain transmission and therapeutic potential of small molecule CB2 receptor agonists, Curr. Med. Chem. 14 (2007) 917–936.
[9] J.C. Ashton, Cannabinoids for the treatment of inflammation, Curr. Opin. Investig. Drugs 8 (2007) 373–384.
[10] G.M. Giblin, C.T. O'Shaughnessy, A. Naylor, W.L. Mitchell, A.J. Eatherton, B.P. Slingsby, D.A. Rawlings, P. Goldsmith, A.J. Brown, C.P. Haslam, N.M. Clayton, A.W. Wilson, I.P. Chessell, A.R. Wittington, Green, R Discovery of 2-[(2,4-dichlorophenyl)amino]-N-[(tetrahydro- 2H-pyran-4-yl)methyl]-4-(trifluoromethyl)- 5-pyrimidinecarboxamide, a selective CB2 receptor agonist for the treatment of inflammatory pain, J. Med.Chem. 50 (2007) 2597–2600.
[11] J. Guindon, A.G. Hohmann, Cannabinoid CB2 receptors: a therapeutic target for the treatment of inflammatory and neuropathic pain, Br. J. Pharmacol. 153 (2008) 319–334.
[12] A.D. Khanolkar, D. Lu, M. Ibrahim, R.I. Duclos, G.A. Thakur, T.P. Malan, F. Porreca, V. Veerappan, X. Tian, C. George, D.A. Parrish, D.P. Papahatjis, A. Makriyannis, Cannabilactones: a novel class of CB2 selective agonists with peripheral analgesic activity, J. Med. Chem. 50 (2007) 6493–6500.
[13] J. Fernandez-Ruiz, J. Romero, G. Velasco, R.M. Tolon, J.A. Ramos, M. Guzman, Cannabinoid CB2 receptor: a new target for controlling neural cell survival? Trends Pharmacol. Sci. 28 (2007) 39–45.
[14] M. Maccarrone, N. Battista, D. Centonze, The endocannabinoid pathway in Huntington's disease: a comparison with other neurodegenerative diseases, Prog. Neurobiol. 81 (2007) 349–379.
[15] D. Centonze, A. Finazzi-Agro, G. Bernardi, M. Maccarrone, The endocannabinoid system in targeting inflammatory neurodegenerative diseases, Trends Pharmacol. Sci. 28 (2007) 180–187.
[16] R.J. McKallip, C. Lombard, M. Fisher, B.R. Martin, S. Ryu, S. Grant, P.S. Nagarkatti, M. Nagarkatti, Targeting CB2 cannabinoid receptors as a novel therapy to treat malignant lymphoblastic disease, Blood 100 (2002) 627–634.
[17] G. Velasco, I. Galve-Roperh, C. Sánchez, C. Blázquez, M. Guzmán, Hypothesis: cannabinoid therapy for the treatment of gliomas? Neuropharmacology 47 (2004) 315–323.
[18] R.G. Pertwee, Cannabinoids and multiple sclerosis, Pharmocol. Therapeut 95 (2002) 165–174.
[19] O. Ofek, M. Karsak, N. Leclerc, M. Fogel, B. Frenkel, K. Wright, J. Tam, M. Attar-Namdar, V. Kram, E. Shohami, R. Mechoulam, A. Zimmer, I. Bab, Peripheral cannabinoid receptor, CB2, regulates bone mass, Proc. Natl. Acad. Sci. U.S.A. 103 (2006) 696–701.
[20] A.I. Idris, R.J. van't Hof, I.R. Greig, S.A. Ridge, D. Baker, R.A. Ross, S.H. Ralston, Regulation of bone mass, bone loss and osteoclast activity by cannabinoid receptors, Nat. Med. 11 (2005) 774–779.
[21] Z.L. Lu, J.W. Saldanha, E.C. Hulme, Seven-transmembrane receptors: crystals clarify, Trends Pharmacol. 23 (2002) 140–146.
[22] O.M. Salo, K.H. Raitio, J.R. Savinainen, T. Nevalainen, M. Lahtela-Kakkonen, J.T. Laitinen, T. Järvinen, A. Poso, Virtual screening of novel CB2 ligands using a comparative model of the human cannabinoid CB2 receptor, J. Med. Chem. 48 (2005) 7166–7171;
T. Tuccinardi, P.L. Ferrarini, C. Manera, G. Ortore, G. Saccomanni, A. Martinelli, Cannabinoid CB2/CB1 selectivity. Receptor modeling and automated docking analysis, J. Med. Chem 49 (2006) 984–994;
S. Durdagi, M.G. Papadopoulos, P.G. Zoumpoulakis, C. Koukoulitsa, T. Mavromoustakos, A computational study on cannabinoid receptors and potent bioactive cannabinoid ligands: homology modeling, docking, de novo drug design and molecular dynamics analysis, Mol. Divers 14 (2010) 257–276.
[23] V. Cherezov, D.M. Rosenbaum, M.A. Hanson, S.G. Rasmussen, F.S. Thian, T.S. Kobilka, H.J. Choi, P. Kuhn, W.I. Weis, B.K. Kobilka, R.C. Stevens, High-resolution crystal structure of an engineered human beta2-adrenergic G protein-coupled receptor, Science 318 (2007) 1258–1265.
[24] V.P. Jaakola, M.T. Griffith, M.A. Hanson, V. Cherezov, E.Y. Chien, J.R. Lane, A.P. Ijzerman, R.C. Stevens, The 2.6 angstrom crystal structure of a human A2A adenosine receptor bound to an antagonist, Science 322 (2008) 1211–1217.
[25] K. Palczewski, T. Kumasaka, T. Hori, C.A. Behnke, H. Motoshima, B.A. Fox, I. Le Trong, D.C. Teller, T. Okada, R.E. Stenkamp, M. Yamamoto, M. Miyano, Crystal structure of rhodopsin: a G protein-coupled receptor, Science 289 (2000) 739–745.
[26] J.M. Frost, M.J. Dart, K.R. Tietje, T.R. Garrison, G.K. Grayson, A.V. Daza, O.F. El-Kouhen, L.N. Miller, L. Li, B.B. Yao, G.C. Hsieh, M. Pai, C.Z. Zhu, P. Chandran, M.D. Meyer, Indol-3-yl-tetramethylcyclopropyl ketones: effects of indole ring substitution on CB2 cannabinoid receptor activity, J. Med. Chem. 51 (2008) 1904–1912.
[27] MOE: Chemical Computing Group Inc. Montreal. H3A 2R7 Canada. http://www.chemcomp.com.
[28] A. Bairoch, R. Apweiler, The SWISS-PROT protein sequence database and its supplement TrEMBL in 2000, Nucleic Acids Res. 28 (2000) 45–48.
[29] H.M. Berman, J. Westbrook, Z. Feng, G. Gilliland, T.N. Beth, H. Weissig, I.N. Shindyalov, P.E. Bourne, The protein data bank, Nucleic Acids Res. 28 (2000) 235–242.
[30] W.D.C.P. Cornell, C.I. Bayly, I.R. Gould, K.M. Merz, D.M. Ferguson, D.C. Spellmeyer, T. Fox, J.W. Caldwell, P.A.J. Kollman, A second generation force field for the simulation of proteins, nucleic acids and organic molecules, J. Am. Chem. Soc. 117 (1995) 5179–5196.
[31] T. Tuccinardi, P.L. Ferrarini, C. Manera, G. Ortore, G. Saccomanni, A. Martinelli, Cannabinoid CB2/CB1 selectivity. Receptor modeling and automated docking analysis, J. Med. Chem. 49 (2006) 984–994.
[32] D.I. Chan, D.P. Tieleman, H.J. Vogel, Molecular dynamics simulations of beta-ketoacyl-, beta-hydroxyacyl-, and trans-2-enoyl-acylcarrier proteins of Escherichia coli, Biochemistry 49 (2010) 2860–2868.
[33] S.J. Marrink, X. Periole, D.P. Tieleman, A.H. de Vries, Comment on 'On using a too large integration time step in molecular dynamics simulations of coarse-grained molecular models, Phys. Chem. Chem. Phys. 12 (2010) 2254–2256.
[34] S. Baoukina, S.J. Marrink, D.P. Tieleman, Lateral pressure profiles in lipid monolayers, Faraday Discuss. 144 (2010) 393–409.
[35] C. Kutzner, D. Van der Spoel, M. Fechner, E. Lindahl, U.W. Schmitt, B.L. De Groot, H.J. Grubmüller, Speeding up parallel GROMACS on high-latency networks, J. Comput. Chem. 28 (2007) 2075–2084.
[36] B. Hess, C. Kutzner, D. Van der Spoel, E.J. Lindahl, GROMACS 4: algorithms for highly efficient, load-balanced, and scalable molecular simulations, Chem. Theory Comput. 4 (2008) 435–447.
[37] W.F. Van Gunsteren, S.R. Billeter, A.A. Eising, P.H. Hunenberger, P. Kruger, A.E. Mark, W.R.P. Scott, I.G. Tironi, Biomolecular simulation, in: The GROMOS96 manual and user guide. Vdf Hochschulverlag AG an der ETH Zurich, 1996, pp. 1–1042.
[38] O. Berger, O. Edholm, F. Jähnig, Molecular dynamics simulations of a fluid bilayer of dipalmitoylphosphatidylcholine at full hydration, constant pressure, and constant temperature, Biophys. J. 72 (1997) 2002–2013.
[39] A.W. Schuettelkopf, D.M.F. Van Aalten, PRODRG – a tool for high-throughput crystallography of protein-ligand complexes, Acta Crystallogr. D 60 (2004) 1355–1363.
[40] J.A. Lemkul, W.J. Allen, D.R. Bevan, Practical Considerations for Building GROMOS-Compatible small molecule Topologies, J. Chem. Inf. Model. 50 (2010) 2221–2235.
[41] J. Wang, W. Wang, P.A. Kollman, D.A. Case, Automatic atom type and bond type perception in molecular mechanical calculations, J. Mol. Graph. Model. 25 (2006) 247–260.
[42] A. Jakalian, B.L. Bush, D.B. Jack, C.I. Bayly, Fast efficient generation of high-quality atomic charges, AM1-BCC Model: Method J. Comput. Chem. 21 (2000) 132–146.
[43] A. Jakalian, D.B. Jack, C.I. Bayly, Fast, efficient generation of high-quality atomic charges. AM1-BCC model: II. Parameterization and validation, J. Comput. Chem. 23 (2002) 1623–1641.
[44] Javier Ramos, Víctor L. Cruz, Javier Martínez-Salazar, Nuria E. Campillo, Juan A. Páez, Dissimilar interaction of CB1/CB2 with lipid bilayers as revealed by

molecular dynamics simulationw, Phys. Chem. Chem. Phys. 13 (2011) 3660–3668.
[45] W. Humphrey, A. Dalke, K. Schulten, VMD: visual molecular dynamics, J. Mol. Graph 14 (1996) 33–38 27-8.
[46] M.G. Wolf, M. Hoefling, C. Aponte-Santamaría, H. Grubmüller, G. Groenhof, g_membed: efficient insertion of a membrane protein into an equilibrated lipid bilayer with minimal perturbation, J. Comput. Chem. 31 (2010) 2169–2174.
[47] U. Essmann, L. Perera, M.L. Berkowitz, T. Darden, H. Lee, L.G. Pedersen, A smooth Particle Mesh Ewald method, J. Chem. Phys. 103 (1995) 8577–8593.
[48] B.J. Hess, P-LINCS: a parallel Linear constraint Solver for molecular simulation, Chem. Theory Comput. 4 (2008) 116–122.
[49] G. Bussi, D. Donadio, M. Parrinello, Canonical sampling through velocity scaling, J. Chem. Phys. 126 (2007) 014101.
[50] H.J.C. Berendsen, J.P.M. Postma, W.F. Van Gunsteren, A. Di Nola, J.R. Haak, Molecular dynamics with coupling to an external bath, J. Chem. Phys. 81 (1984) 3684–3690.
[51] W.L. DeLano, The PyMOL molecular graphics system DeLano Scientific. San Carlos, CA, USA, 2002.http://www.pymol.org.
[52] R.D. Cramer III, D.E. Patterson, J.D. Bunce, Prog. Clin. Biol. Res. 291 (1989) 1–165.
[53] G. Klebe, U. Abraham, T. Mietzner, Molecular similarity indices in a comparative analysis (CoMSIA) of drug molecules to correlate and predict their biological activity, J. Med. Chem. 37 (1994) 4130–4146.
[54] Sybyl X 1.0 Tripos Inc 1699 South Hanley Road. St Louis. Missouri. 63144. USA 25.
[55] A. Ranise, S. Cesarini, A. Spallarossa, F. Sancassan, F. Bondavalli, O. Bruno, S. Schenone, G. Menozzi, P. Fossa, L. Mosti, Unprecedented one-pot stereoselective synthesis of Knoevenagel-type derivatives via in situ condensation of N-methyleniminium salts of ethylenethiourea and ethyleneurea with active methylene reagents, Synthesis-Stuttgart 16 (2007) 2495–2502.
[56] E. Cichero, S. Cesarini, L. Mosti, P. Fossa, CoMFA and CoMSIA analyses on 1,2,3,4-tetrahydropyrrolo[3,4-b]indole and benzimidazole derivatives as selective CB2 receptor agonists, J. Mol. Model. 16 (2010) 1481–1498.
[57] D. Pagé, H. Yang, W. Brown, C. Walpole, M. Fleurent, M. Fyfe, F. Gaudreault, St-Onge S New 1,2,3,4-tetrahydropyrrolo[3,4-b]indole derivatives as selective CB2 receptor agonists, Bioorg. Med. Chem. Lett. 22 (2007) 6183–6187.
[58] D. Pagé, E. Balaux, L. Boisvert, Z. Liu, C. Milburn, M. Tremblay, Z. Wei, S. Woo, X. Luo, Y.X. Cheng, H. Yang, S. Srivastava, F. Fhou, W. Brown, M. Tomaszewski, C. Walpole, L. Hodzic, S. St-Onge, C. Godbout, D. Salois, K. Payza, Novel benzimidazole derivatives as selective CB2 agonists, Bioorg. Med. Chem. Lett. 13 (2008) 3695–3700.